# AERODYNAMICS OF TACTICAL WEAPONS

# TO MACH NUMBER 8 AND ANGLE-OF-ATTACK OF 180° (U)

L. Devan
L. A. Mason
F. G. Moore

Naval Surface Weapons Center, Dahlgren, Virginia

## ABSTRACT

The NSWC Aeroprediction Code has been extensively applied to the prediction of static and dynamic aerodynamics of missile configurations. Major extensions have recently been made to the code to extend its capability to $0 \leq M_\infty \leq 8$ and $0° \leq \alpha \leq 180°$ and also to improve the transonic inviscid body alone static aerodynamic predictions and the dynamic derivative predictions for all Mach numbers. The theoretical basis for the code extensions are outlined and previous methods are briefly reviewed. The code is evaluated through comparisons of computational examples with experiment for body alone, body-tail and body-tail-canard configurations. The speed and accuracy of the code are ideal for use in preliminary design. Examples of design applications to specific tactical weapon configurations are presented.

## INTRODUCTION

A continuous need exists for estimating the aerodynamic characteristics of a wide variety of tactical missile and projectile configurations, especially in the preliminary or conceptual design phase. To meet this need, the Navy (in cooperation with the Army) undertook the development of a rapid, inexpensive, easy to use Aerodynamic Prediction Code in 1971. The code was developed so as to handle fairly general wing-body-tail configurations and hence have direct application to a high percentage of tactical weapon designs. Preliminary versions of the code were published in 1972, 1975, and 1977. The changing mission requirements for both current and future weapons has dictated, however, the need to revise and extend the capabilities of the 1977 version of the Aeroprediction Code, which was limited to $M_\infty \leq 3.0$ and small angles-of-attack ($\alpha \leq 15°$), to higher Mach numbers and angles-of-attack.

The objective of the current effort, which is nearing completion, is to extend the 1977 version of the Aeroprediction Code to $M_\infty = 8$ and $\alpha = 180°$. In addition, modification of some of the existing methods due to advances in the state-of-the-art and computer program optimization is desirable.

The general approach of the code development has been to combine existing and newly developed computational methods into a single computer program. The basic method is that of component superposition where the body-alone, lifting-surface-alone and interference contributions are added to obtain total configuration aerodynamics. The code development has occurred in four increments. The first three of these increments were previously reported, and led to the development of a code capable of determining the aerodynamic coefficients for axisymmetric, non air-breathing configurations with up to two sets of lifting surfaces for low angles-of-attack and Mach numbers to 3.0. The results of the fourth increment, required to meet the stated objective, is the subject of this paper. Program plans for this effort and some early results were presented at the 11th Naval Symposium on Ballistics.[1] The theories used, outlined briefly here, are discussed in more detail elsewhere.[5,6] The resulting code has computational times, required for the estimate of static and dynamic aerodynamic coefficients for a body-tail-canard configuration for one freestream condition, that are in CPU seconds on a CDC 6700 computer as opposed to minutes or hours often required for more detailed physical and numerical models. The accuracy obtained, however, is compatible with that required for preliminary or intermediate design estimates.

Numerous computations for a variety of configurations have been attempted on the Extended Aeroprediction Code and the results compared with available data. Representative comparisons with experiment used in evaluating the code and sample applications illustrating the use of the code to achieve improved performance will be discussed in a later section.

## CONFIGURATIONAL GEOMETRY AND FREESTREAM CONDITIONS

The most complex configuration considered is illustrated in Figure 1. The body may be pointed, spherically blunted or truncated. The remainder of the body may consist of one or two piecewise continuous nose sections, a constant crossection afterbody, and a boattail or flare. The wing or canard fins have a trapezoidal planform with a biconvex or modified double-wedge crossection and sharp or spherically blunted leading and trailing edges. Tip edges are assumed parallel to the freestream at zero angle-of-attack. Fin crossections are piecewise similar with span. No camber, twist, dihedral, or airfoil distortion is considered. Lifting surface sets are planar or cruciform. Horizontal, all-movable control deflections in the plus position are considered. Canard/wing and tail fin sets are aligned.

For various Mach number and angle-of-attack regions there are geometric restrictions. These will be elaborated upon in later sections.

Freestream condition description consists of Mach number, Reynolds number per foot per Mach number, and angle-of-attack. Roll orientation is considered at higher angles-of-attack only. Inlet and exhaust plume effects are not considered.

## SUMMARY OF ANALYSIS METHODS

The analysis methods will be discussed in general terms. For more detailed theoretical discussions and derivations of the individual methods, the reader is referred to reports currently published as well as those in publication (References 2-7, 9).

BODY-ALONE STATIC METHODS

The body-alone low angle-of-attack static prediction methods[2-5] are summarized in Figure 2. The transonic nose pressure drag and body inviscid normal force methods were modified under contract to NEAR, Inc., with additional modifications accomplished in-house. The second-order shock-expansion extension work was accomplished under contract by Professor F. DeJarnette of North Carolina State University.

The transonic/subsonic nose wave drag prediction assumes that the nose, boattail, and base are aerodynamically isolated. This assumes the existance of a minimum length afterbody. The nose shape is assumed to be a spherically blunted tangent ogive or a spherically blunted cone. To obtain results for a more general nose shape, linear interpolations between the tangent ogive and the cone pressure drag predictions are made using the initial body slope at the sphere-nose junction and the nose-afterbody slope. Thus, for a zero shoulder slope, the tangent ogive value is computed and for equal values of initial and final slope values, the cone value is computed. The tangent ogive pressure drag prediction is based upon interpolation in a table of values of Mach number, $M_\infty$ ; nose length, $L_N$; and nose spherical radius, $R_N$. Ranges of values are $.8 \leq M_\infty \leq 1.2$, $.75 < L_N < 5.0$ calibers, and $0. < R_N < .5$ calibers. The majority of the pressure drag data was generated by solving the Euler equations by an unsteady implicit time asymptotic method. A portion of the data was generated by solution of the full potential equation by the method of South and Jameson. Below $M_\infty = .8$ the pressure drag is decayed quadratically to zero at $M_\infty = .5$. The cone pressure drag is obtained from a blend of integrated pressure data and Taylor-Maccoll solutions. The pressure drag is obtained as an interpolation in a table of values of $M_\infty$ versus cone angle, $\delta$ (bluntness is neglected). Ranges of values are $.5 < M_\infty < 1.2$, $0 < \delta < 20°$. Below $M_\infty = .5$ an asymptotic value is assumed. The boattail wave drag is based upon small disturbance solutions assuming a long afterbody for $1.05 < M_\infty < 1.2$. Below $M_\infty = 1.05$ the boattail drag is decayed linearly to zero at $M_\infty = .95$.

The transonic/subsonic normal force prediction is for $0 < M_\infty < 1.2$. The new transonic normal force prediction is based on a combination interpolation and least squares curve fit in Mach number and geometric parameters. The nose is a blunted tangent ogive. Other body parameters are afterbody length, boattail angle, and boattail length. Parameter limits are $0 < R_N < .5$ calibers, $1.5 < L_N < 5.0$ calibers, $0 < L_A$ (afterbody length) $< 5.0$ calibers, $0 < L_B$ (boattail length) $< 2.0$ calibers, and $0 \leq \theta_B \leq 10°$ for the conical boattail angle. Values of $C_{N\alpha}$ and $C_{M\alpha}$ (about the nose) are obtained by solving the Euler equations at 1° by an unsteady implicit time asymptotic method at $M_\infty = .75, .90, .95$ and 1.2. Currently prediction values at $M_\infty = .6$ are given by the earlier model and at $M_\infty = 1.2$ by a low supersonic Mach number potential model. Interpolation provides a solution for $.6 < M_\infty < 1.2$. Below $M_\infty = .6$, the earlier model was used. Currently the new algorithm is an input choice to the program since neither method is particularly satisfactory over the full range of conditions.

The small disturbance potential solutions for the low supersonic range are applicable from $1.2 < M_\infty < M_\ell$; $M_\ell$, a program input, is chosen between 2 and 3.5 depending on nose shape and whether or not lifting surfaces are also present. A high supersonic prediction method is used for $M_\infty > M_\ell$. The method used is a modified version of the second-order shock-expansion method which predicts inviscid static coefficients with good accuracy for bodies with short afterbodies and a flare. The wave drag predicted is adequate for nose-afterbody

configurations but is poorer for bodies with a boattail. The normal force prediction is fair for nose-afterbody configurations, and again is poorer for bodies with negative slopes. The pitching moment prediction in general is poorer not only for the higher Mach numbers but is a weakness of all of the methods available over the entire Mach number range.

## LIFTING SURFACE AND INTERFERENCE STATIC METHODS

Lifting surface and interference methods are summarized in Figure 3. The high supersonic methods were developed by Professor F. DeJarnette.

Above $M_\infty = M_\ell$, a shock-expansion strip estimate is used. First the angle between the local surface normal and the free stream velocity is found. A local oblique shock value is used for compression angles and a local Prandtl-Meyer value is used for expansion angles. The pressure distribution is independent of span since similarity of crossection is assumed. For a blunt leading edge a modified Newtonian distribution is assumed. As Mach number and aspect ratio increase the wing-alone prediction improves. However, interference effects are neglected.

The methods used at lower Mach numbers were previously documented.[3] For the symmetric low supersonic drag problem no swept forward trailing edge is permitted. This is a numerical method restriction rather than a physical restriction. For the low supersonic lift problem no subsonic trailing edge is allowed. In addition, the zone of influence must not include the opposite tip edge of a two fin planform. For the drag problem, the trailing edge sweep angle is cut off at 0°. For the lifting problem the Mach number is kept just above or at the critical Mach number.

## METHODS FOR COMPUTING DYNAMIC DERIVATIVES

Methods for computing dynamic derivatives are summarized in Figure 4.

For the fourth increment in the code development process, improvements and extensions were made in the pitch and roll damping prediction method.

Dr. L. Ericsson of Lockheed Missiles and Space Company, under contract to NSWC, was responsible for developing a method to improve the prediction of pitch damping for small angles of attack. In the low supersonic region the method is restricted by the slender wing-body analysis. It is assumed that the slender-wing body analysis is usable to $M_\infty = 2$. At this condition the aspect ratio of the tail is restricted to less than 2.3. The current theory is restricted to body-tail configurations. For the body-alone prediction, when the LMSC model deviates too greatly from the older, empirical G.E. SPINNER code prediction, the SPINNER prediction is selected. Currently the use of the LMSC algorithm is a code input option. For body-canard-tail configurations only the body-alone prediction is utilized.

For the earlier methods used in the code the same restrictions on Mach number, which prevent trailing edge subsonic conditions or the opposite side edge lying in the zone of influence, which were made for the lifting surface-alone normal force problem, again apply. For the lifting surface-body problem

the planform considered is that obtained by extending the leading and trailing edges to the body centerline.

Improvements were also made in the method of computing the transonic empirical roll and pitch damping for configurations with lifting surfaces. At high Mach numbers above $M_\infty = M_\ell$, a strip method, based on the static normal force strip loading, is used to predict roll and pitch damping for configurations with lifting surfaces. Thus, two methods are available for predicting pitch damping for the entire Mach number regime.

## HIGH ANGLE-OF-ATTACK STATIC AERODYNAMICS

The method used in the code is a direct adaption of the empirical methodology of Reference 7. Restrictions of this code are:

(1) Mach number: .8 to 3.0.

(2) Angle-of-attack: 0° to 180° for isolated components (plus position) and 0° to 45° for body-tail combinations and roll angles 0° to 180°.

(3) Tail: Trapezoidal plan form, edge parallel to body centerline

(a) Leading edge sweep angle: 0 to 70 degrees

(b) Taper ratio: 0 to 1.

(c) Aspect ratio (two fins): .5 to 2.0.

(d) No control deflection

(e) Tail trailing edge: sweep zero and parallel to body base.

(4) Nose length (pointed tangent ogive): 1.5 to 3.5 calibers.

(5) Cylindrical afterbody 6 to 18 calibers long.

(6) Total span to diameter ratio (two fins): 1 to 3 1/3.

Body alone and body-tail normal force and $X_{cp}$ are predicted as a function of Mach number, roll angle, and angle of attack. In addition, the roll moment is also predicted.

## ANALYSIS EVALUATION AND SAMPLE COMPUTATIONS FOR NEW CODE ELEMENTS

This section will present examples illustrating both the strengths and the weaknesses of the new methods adapted and integrated into the NSWC code. The reader should remember that all of the new methods met our accuracy requirements <u>in general</u> over the range of applicability although in some individual cases shown, the accuracy was poorer.

An illustration of the capability of the new High Mach number routine is given in Figures 5-7. Here the body alone static aerodynamic predictions of

the current routine are compared to integrated pressure data and the small disturbance potential codes[1,8] for a blunted, tangent ogive nose, 6.0 caliber afterbody configuration. Above $M_\infty = 1.5$, the comparison of the High Mach prediction with data is quite good for the forebody drag, $C_{AF}$ (wave drag plus friction drag) while the normal force, $C_{N\alpha}$, and center-of-pressure, $X_{cp}$, predictions are shown to degrade somewhat. In general, the predictions improve with increasing nose length and Mach number (although this was not shown for this case due to a lack of data). In Figure 8, comparisons are shown for a NASA flared body. Small modifications were necessary to the body geometry to make it compatible with the input requirements of the computer code. As a result, the agreement in general is only fair except for $C_{N\alpha}$ at the higher Mach numbers where the agreement is good. In general, the $C_{N\alpha}$ prediction will be poorer for bodies with negative slopes (i.e. boattails). It is also shown that $X_{cp}$ is rather poorly predicted by all three computational methods.

In Figures 9 and 10 are shown comparisons of the shock-expansion strip theory for wings with the low Mach number small disturbance estimates. For larger aspect ratios and higher Mach numbers (smaller zones of influence) the comparison is improved. No interference is considered for $M_\infty > M_\ell$. However, the $C_{N\alpha}$ prediction is generally on the high side which partially compensates for this omission In these examples $\Lambda_1$ is the leading edge sweep, $A_w$ is the aspect ratio and $\lambda_w$ is the taper ratio. The wing crossection is that of a symmetric diamond.

Figures 11 and 12 illustrate applications of the code to body-canard-tail and body-wing configurations. Data for the TMX-1751 configuration include the contributions of body strakes (not shown in the sketch). These strakes were not included in the model,due to limits on the number of lifting surfaces and the small aspect ratio,which partially accounts for the $C_{N\alpha}$ and $X_{cp}$ differences. The comparison is good for the TMX-187 configuration with the flared afterbody.

Figures 13-16 illustrate the capabilities of the adapted Martin High angle-of-attack empirical algorithm. The slope and magnitude of the $C_N$ predictions compare quite well. However, the $X_{cp}$ and $C_\ell$ predictions are of the right order of magnitude only, except at fairly high angles-of-attack where the predictions improve markedly for the lower Mach numbers.

As previously indicated, the modified LMSC dynamic derivatives model occasionally experiences a total breakaway from the data for body alone configurations. This problem is illustrated in Figure 17 for the Army-Navy Spinner configuration. As a result, the current combined code compares the LMSC model predictions with the G.E. SPINNER code prediction. If the deviation is large, as in this case, the SPINNER prediction is selected. In Figure 18, the relative capabilities of the older pitch damping prediction method, the LMSC model and the strip theory are shown for the Basic Finner configuration. The strip theory is seen to be quite adequate at the higher Mach numbers for predicting both the pitch damping and the roll damping coefficient, $C_{\ell_p}$ (see Figure 19). The overall agreement of the new method for all Mach numbers is considered to be good.

The relative improvement in the transonic predictions is illustrated in Figures 20-23. In Figure 20, the computed transonic nose wave drag for the M-117 Bomb is compared with data. For this case, the NEAR algorithm is shown to improve the estimate somewhat. The experimental pressure data, however, was

somewhat sparse for an accurate numerical integration. The improvement is much more obvious in Figure 21 which shows a comparison of the NEAR algorithm prediction and older theory with data for blunted tangent ogive-cylinders with 6.0 caliber afterbodies. However, there is no apparent improvement in the prediction for $C_{N_\alpha}$ and $X_{cp}$ in the transonic flow regime as shown in Figures 22 and 23. Neither method seems to be particularly outstanding. (A more thorough evaluation is present in Reference 5.)

## SPECIAL CODE FEATURES

The Aeroprediction Code which applies the methodology previously indicated in Figures 2-4 and the High Angle-of-Attack algorithm, has been updated to include the new methodology presented. (Details of the earlier version of the code are available in Reference 9). In addition to the new computational methods, other elements of the code have been corrected and improved. For example, the data input and output have been extensively changed to simplify and clarify those aspects of the program and to optimize the code for the user. For example, the wing or tail input data consists of the minimum required for the computations and yet allows considerable detail to be given. The body-along geometry is described by the number of points on the body surface for each piecewise continuous segment, a single logic variable, and body surface coordinates. The description is basically independent of Mach number with only minor exceptions. The program has been segmented in order to minimize the storage required for loading. Currently, the code requires 160K octal central memory or less. For more universal use, all FORTRAN statements will be standard ANSI format or machine independent. For missile design, the output has been expanded to include the pitching moment coefficient components about the given moment center and the normal force/pitching moment dependencies on angle-of-attack and control deflections. Thus, for the entire configuration, the normal force coefficient for a given Mach number can be described as

$$C_N = \alpha \left(C_{N_\alpha} + C_{N_{\alpha\alpha}} \alpha\right) + C_{N_{\delta_t}} \delta_t + C_{N_{\delta_c}} \delta_c$$

where $\delta_c$ and $\delta_t$ are the canard and tail control deflections, respectively, and $C_{N_{\alpha\alpha}}$ is the body viscous crossflow term. The expression is similar for the moment coefficient. Utilizing these outputs one can obtain the hinge moments and other coefficients needed for a linear aerodynamic performance analysis of a missile configuration.

## APPLICATIONS TO DESIGN

The Aerodynamic Prediction Code has been extensively applied to the design of both conventional and unconventional tactical weapons. To conserve space, only a few specific examples are shown here which hopefully will provide some indication of the code's flexibility. Many more examples will be given in the design manual to be published later this year (Reference 6).

## PROJECTILE PERFORMANCE OPTIMIZATION

The objective of this study was to optimize the performance of a full-bore, axisymmetric projectile to obtain the minimum time-of-flight and highest terminal velocity at a given range with no degradation in accuracy. This was to be accomplished by optimizing the shape to minimize the total drag, through determination of the best weight to obtain the optimum ballistic coefficient and by judicious selection of the center-of-gravity location. An optimization scheme developed by Hagar, et al.[10] (which has since been upgraded by Moga[11]) indicated that for a five caliber body, the minimum drag profile would be similar to that shown in the top corner of Figure 24. Methods to quickly predict the aerodynamics of this profile are more limited than one might at first suppose, particularly with respect to the two-third power law nose contour and the 1.8 caliber boattail. For instance, the range of applicability of the DATCOM is for boattail lengths greater than 2.0 calibers and tangent or conical nose shapes. The G.E. SPINNER code includes data for some secant ogive nose shapes which can closely approximate the two-third power law nose but is limited to boattail lengths of less than 1.0 calibers. The small afterbody length (approximately .05 calibers) also restricted the use of additional methods and data. The Aeroprediction Code was utilized to obtain the static aerodynamic coefficients for this configuration so initial estimates of its stability could be made. Using these initial estimates, the design was fabricated and successfully flown in the 30 MM caliber size. Comparisons of the theory with the ballistic range data later obtained for the design are given in Figure 24. Good agreement was obtained in each case. As a result, the predicted values could then be used to conduct a stability analysis throughout the trajectory with greater confidence. Use of the Aeroprediction Code therefore allowed the designer to eliminate expensive wind tunnel tests and the bulk of ballistic range tests, even though extensive changes in the design were made, and demonstrate the benefits of the proposed design. The improvements in this case were substantial as shown in Table I below.

Table 1. Benefits of the 30 MM Optimal Projectile*

| | 30 MM Standard | 30 MM Optimal | Improvement |
|---|---|---|---|
| Range (KM) | 3.0 | 3.0 | --- |
| Average $C_D$ | .36 | .22 | 39% |
| Time-of-Flight (sec) | 5.70 | 3.86 | 32% |
| Terminal Velocity (FPS) | 967 | 1559 | 61% |
| Accuracy (rad. std. dev., mts) | .6 | .65 | --- |

* Computer generated trajectory based on experimental drag data.

## STRUCTURAL ANALYSIS

An example of application toward structural design was presented at the

11th Navy Symposium on aeroballistics.[1] As indicated in the previous paper, the Aeroprediction Code was modified to compute the total sectional normal force coefficients along the body as a function of Mach number and angle-of-attack. The results were then used in the structural analysis. The results of the analysis, repeated here in Figure 25, indicate that structural failure of the two configurations examined could occur during maneuvering flight due to the large aerodynamic bending moment. Flight tests confirmed the prediction and the design was successfully modified.

## MISSILE CONTROL DESIGN

The use of the code in preliminary missile design was recently illustrated for the Advance Point Defense System (APODS) missile concept. The guided APODS missile is currently an 18.0 caliber design with a 2.0 caliber Van Kármán ogive radome, a 16.0 caliber afterbody and four cruciform tail fins for control (see Figure 26). In order to obtain an estimate of its performance capabilities and determine the optimum control gains, the Aeroprediction Code was utilized to provide the static aerodynamics at angle-of-attack and the moment contributions relative to the center-of-gravity. The estimated static and dynamic aerodynamic coefficients for the APODS missile are given in Figure 27. These results were fed into the computer guidance model. A sample trajectory and the tail control autopilot response are shown in Figures 28 and 29, respectively. Results such as these can then guide the design in modifying the configuration or the control gains to maximize performance.

## SUMMARY

An Extended Aerodynamic Prediction Code for rapid, approximate estimates of the static and dynamic coefficients for guided and unguided tactical weapons has been developed. The range of applicability of the code is $0 \leq M_\infty \leq 6.0$ (up to $M_\infty = 8.0$ for certain body alone cases) and $0° \leq \alpha \leq 45°$ (up to $\alpha = 180°$ for computing the drag on certain body alone configurations). A large number of configurations can be accurately modeled on the program. Final verification of the predictions is nearing completion. The code, accompanied by a Design Manual and a User's Guide, is scheduled for release in the fourth quarter of FY81.

## REFERENCES


1. J. Sun, L. Devan, N. J. Moga, and F. G. Moore,"Aerodynamic Prediction for Tactical Weapons,"presented at the 11th Naval Symposium on Aeroballistics, 22-24 August 1978, Philadelphia, PA, Proceedings, Vol. I, pp 1-31.

2. F. G. Moore, Body Alone Aerodynamics of Guided and Unguided Projectiles at Subsonic, Transonic, and Supersonic Mach Numbers, NWL TR-2796, November 1972.

3. F. G. Moore, Aerodynamics of Guided and Unguided Weapons Part I - Theory and Application, NWL TR-3018, December 1973.

4. F. G. Moore and R. C. Swanson, Jr., Aerodynamics of Tactical Weapons to Mach Number 3 and Angle-of-Attack 15°: Part I - Theory and Application, NSWC/DL TR-3584, February 1977.

5. L. Devan, Aerodynamics of Tactical Weapons to Mach Number 3 and Angle-of-Attack 180°, NSWC TR 80-346, October 1980.

6. L. Devan, L. Mason, D. McMillan, and F. Moore, Aerodynamic Design Manual for Tactical Weapons, NSWC Report in Progress, 1981.

7. G. F. Aiello, Aerodynamic Methodology (Bodies with Tails at Arbitrary Roll Angles, Transonic and Supersonic), Martin Marietta Corp., OR 14, 145, Orlando, FL, April 1976.

8. L. Devan,"An Improved Second-Order Theory of Inviscid Supersonic Flow Past Bodies of Revolution,"Paper 80-0030, presented at the AIAA 18th Aerospace Sciences Meeting, Pasadena, CA, January 1980.

9. R. C. Swanson, Jr., and F. G. Moore, Aerodynamics to Mach Number 3 and Angle of Attack 15°, Part II - Computer Program and Usage, NSWC/DL TR-3600, March 1977.

10. W. W. Hager, F. R. DeJarnette, and F. G. Moore, Optimal Projectile Shapes for Minimum Total Drag, NSWC TR-3597, Dahlgren, VA, May 1977.

11. N. J. Moga, Optimal Bodies for Minimum Total Drag at Supersonic Speeds, NSWC TR-80-208, Dahlgren, VA, May 1980.

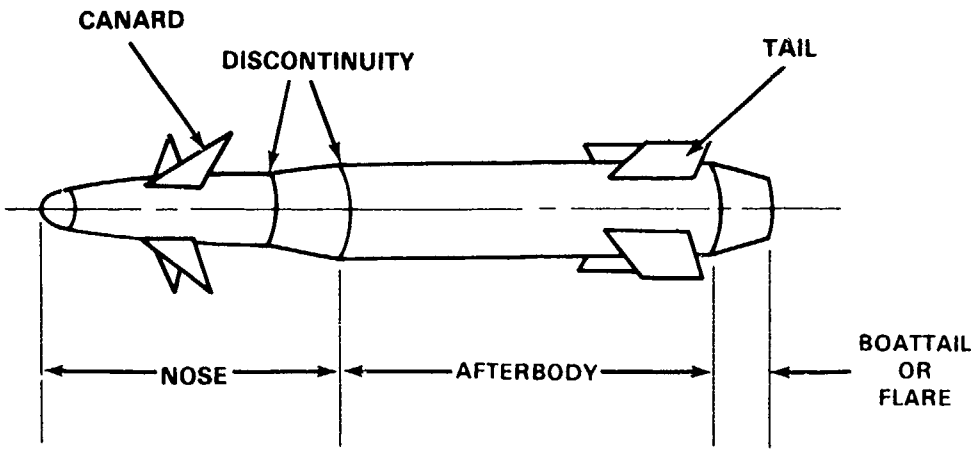


Figure 1. Configuration Geometry

| COMPONENT \ MACH NUMBER REGION | SUBSONIC | TRANSONIC | LOW SUPERSONIC | HIGH SUPERSONIC |
|---|---|---|---|---|
| NOSE WAVE DRAG | – | EULER PLUS EMPIRICAL | SECOND-ORDER VAN DYKE PLUS MODIFIED NEWTONIAN | SECOND-ORDER SHOCK-EXPANSION PLUS MODIFIED NEWTONIAN |
| BOATTAIL WAVE DRAG | – | WU AND AOYOMA | SECOND-ORDER VAN DYKE | SECOND-ORDER SHOCK-EXPANSION |
| SKIN FRICTION DRAG | VAN DRIEST II | | | |
| BASE DRAG | EMPIRICAL | | | |
| INVISCID LIFT AND PITCHING MOMENT | EMPIRICAL | EULER OR WU AND AOYOMA PLUS EMPIRICAL | TSIEN FIRST-ORDER CROSSFLOW | SECOND-ORDER SHOCK-EXPANSION |
| VISCOUS LIFT AND PITCHING MOMENT | ALLEN AND PERKINS CROSSFLOW | | | |

Figure 2. New Methods for Computing Body-Alone Aerodynamics

| COMPONENT \ MACH NUMBER REGION | SUBSONIC | TRANSONIC | LOW SUPERSONIC | HIGH SUPERSONIC |
|---|---|---|---|---|
| INVISCID LIFT AND PITCHING MOMENT | LIFTING SURFACE THEORY | EMPIRICAL | LINEAR THEORY | SHOCK-EXPANSION STRIP THEORY |
| WING-BODY INTERFERENCE | SLENDER BODY THEORY AND EMPIRICAL | | LINEAR THEORY, SLENDER BODY THEORY AND EMPIRICAL | — |
| WING-TAIL INTERFERENCE | LINE VORTEX THEORY | | | — |
| WAVE DRAG | — | EMPIRICAL | LINEAR THEORY + MODIFIED NEWTONIAN | SHOCK-EXPANSION + MODIFIED NEWTONIAN STRIP THEORY |
| SKIN FRICTION DRAG | VAN DRIEST | | | |
| TRAILING EDGE SEPARATION DRAG | EMPIRICAL | | | |
| BODY BASE PRESSURE DRAG CAUSED BY TAIL FINS | EMPIRICAL | | | |

Figure 3. New Methods for Computing Wing-Alone and Interference Aerodynamics

| COMPONENT \ MACH NUMBER REGION | SUBSONIC | TRANSONIC | LOW SUPERSONIC | HIGH SUPERSONIC |
|---|---|---|---|---|
| BODY-ALONE PITCH DAMPING MOMENT | EMPIRICAL (OR) MODIFIED SLENDER-BODY THEORY | (OR) LINEAR INTERPOLATION | (OR) EMBEDDED NEWTONIAN THEORY | * |
| WING AND INTERFERENCE ROLL DAMPING | LIFTING SURFACE THEORY | EMPIRICAL | LINEAR THIN-WING THEORY | STRIP THEORY |
| BODY-ALONE MAGNUS MOMENT | EMPIRICAL | | | |
| WING AND INTERFERENCE MAGNUS MOMENT | ASSUMED ZERO | | | |
| BODY-ALONE ROLL DAMPING MOMENT | EMPIRICAL | | | |
| WING AND INTERFERENCE PITCH DAMPING MOMENT | SLENDER-WING THEORY (OR) LIFTING SURFACE THEORY | SUPERSONIC SLENDER-WING THEORY (OR) EMPIRICAL | EMBEDDED NEWTONIAN STRIP THEORY (OR) LINEAR THIN-WING THEORY | ** (OR) STRIP THEORY |

* INPUT OPTION. MACH DIVISION POINTS ARE AT $M_\infty = 1$ AND $M_\infty = \bar{M}^*$. $\bar{M}^*$ IS VARIABLE, BUT $\bar{M}^* \geq 1.5$.

** INPUT OPTION. MACH DIVISIONS AT $M_\infty = 1$ AND A MACH NUMBER DEPENDENT ON ASPECT RATIO, $M_\infty = \sqrt{1 + (A_W/4)^{-2}}$.

Figure 4. New Methods for Computing Dynamic Derivatives

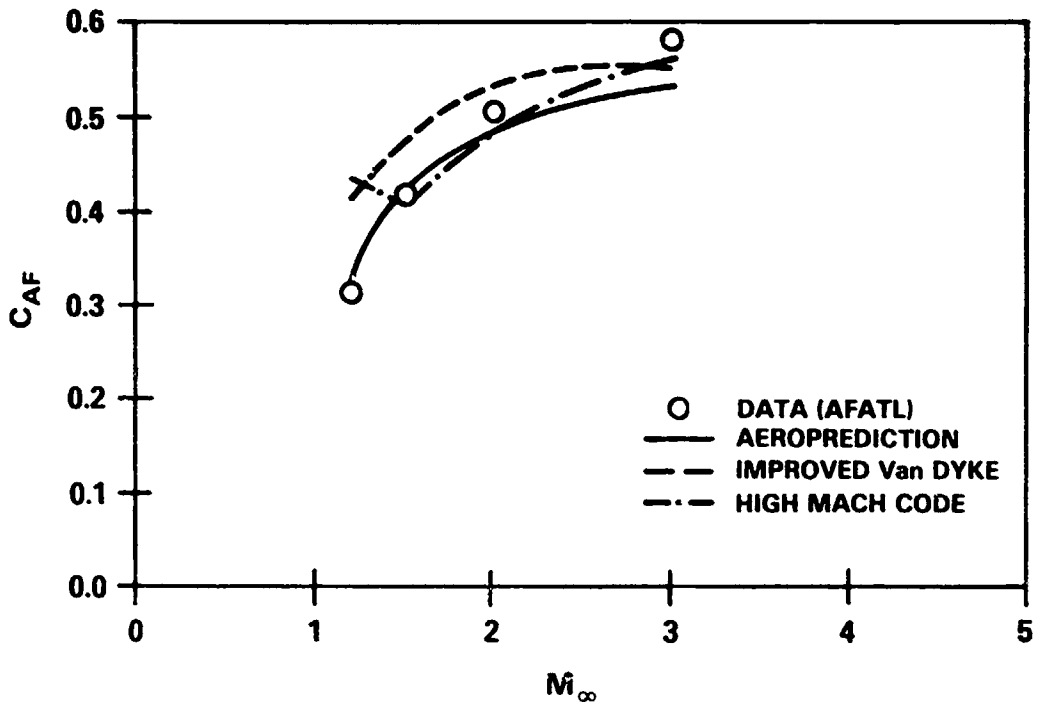


(a) $L_N = 1.859$, $R_N = 0.375$, $\alpha = 0$

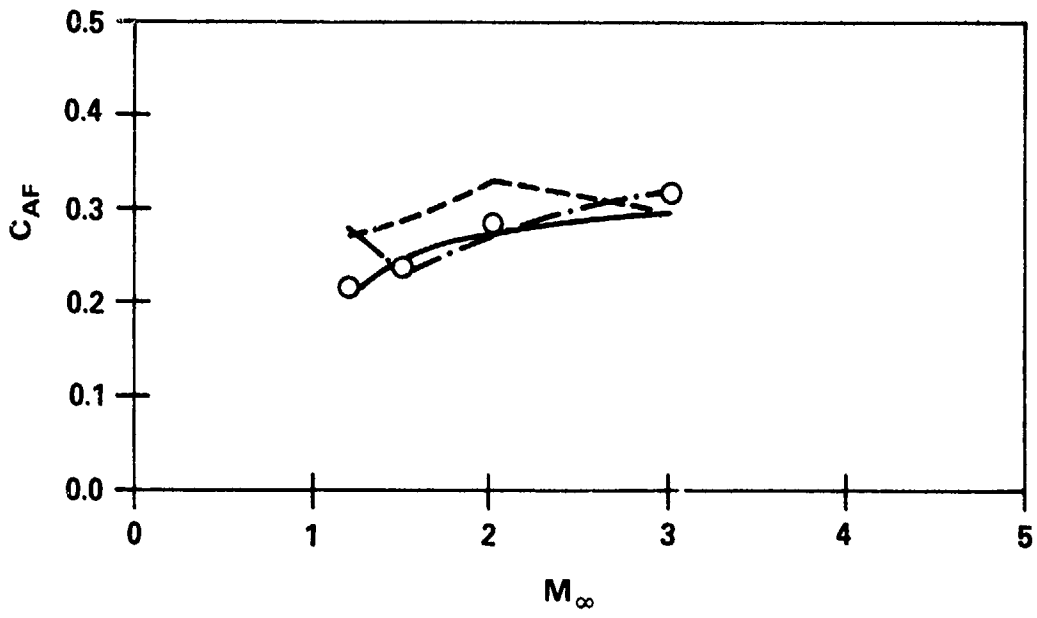


(b) $L_N = 2.357$, $R_N = 0.250$, $\alpha = 0$

Figure 5. Blunted Tangent Ogive-Forebody Axial Force

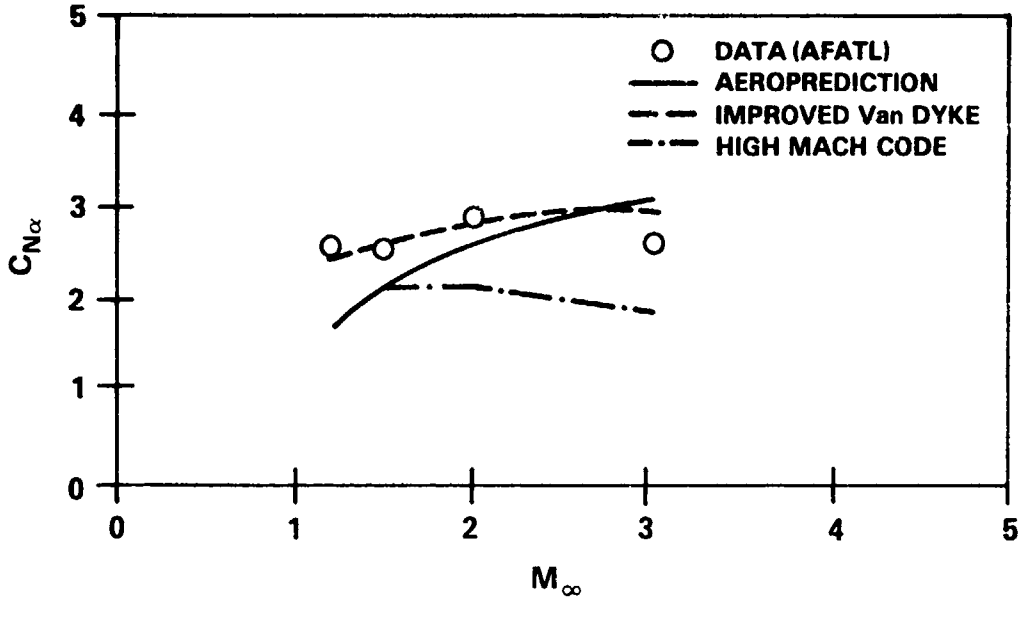


(a) $L_N = 1.859$, $R_N = 0.375$, $\alpha = 0$

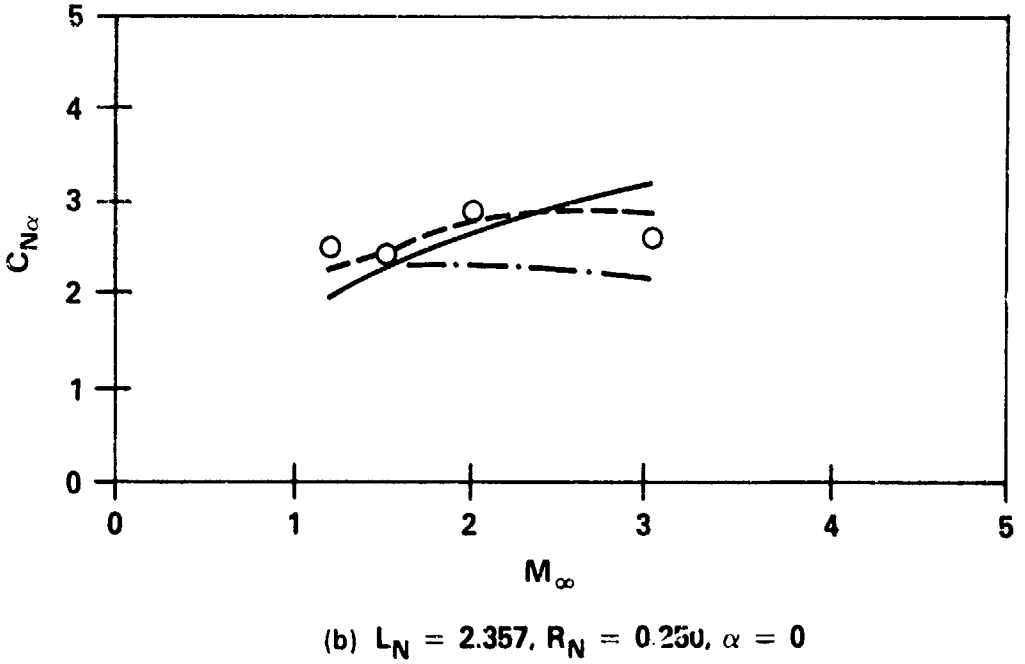


(b) $L_N = 2.357$, $R_N = 0.250$, $\alpha = 0$

Figure 6. Blunted Tangent Ogive-Cylinder, $C_{N\alpha}$

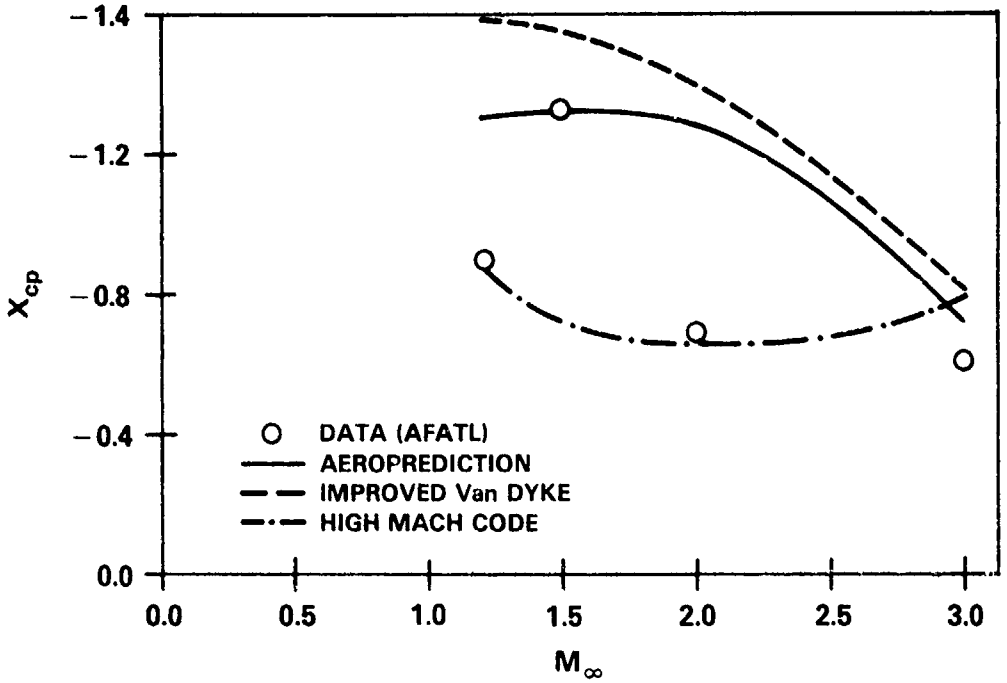


(a) $L_N = 2.357$, $R_N = 0.250$, $\alpha = 0$

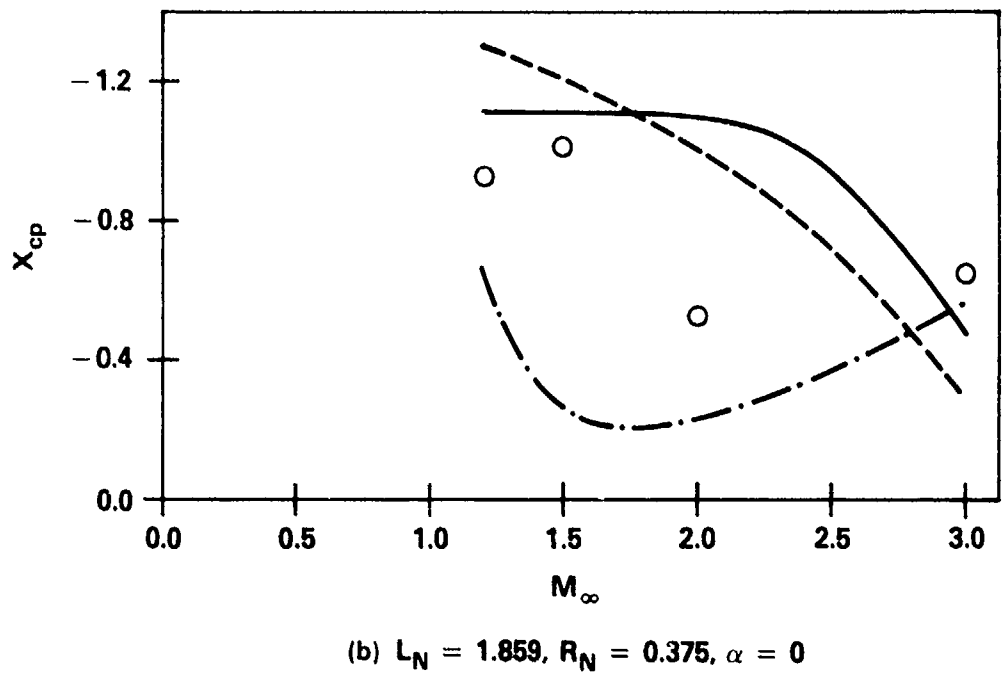


(b) $L_N = 1.859$, $R_N = 0.375$, $\alpha = 0$

Figure 7. Blunted Tangent Ogive-Cylinder, $X_{cp}$ (From Body-Nose Junction)

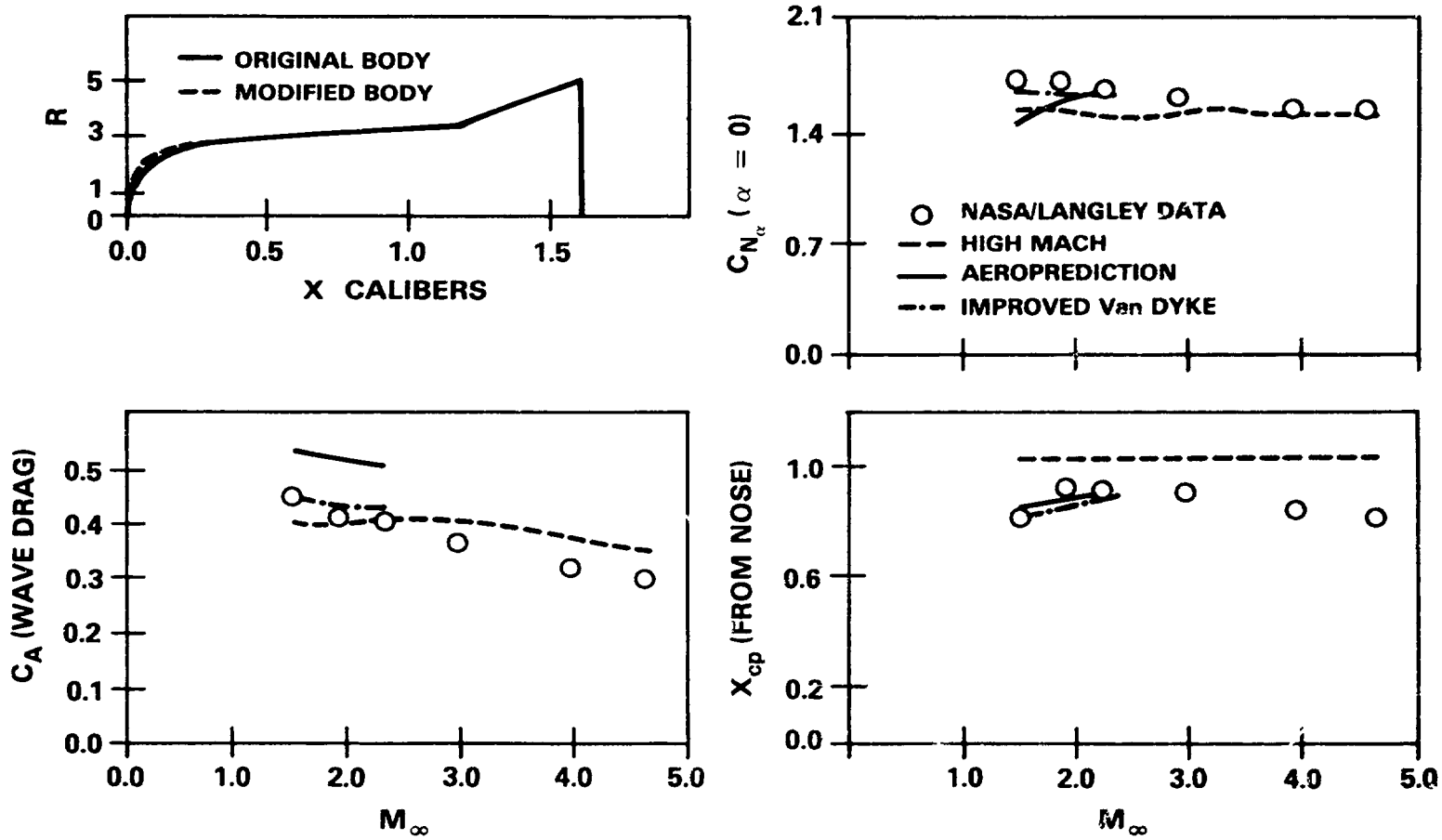


Figure 8. NASA Flared-Body Data Comparison

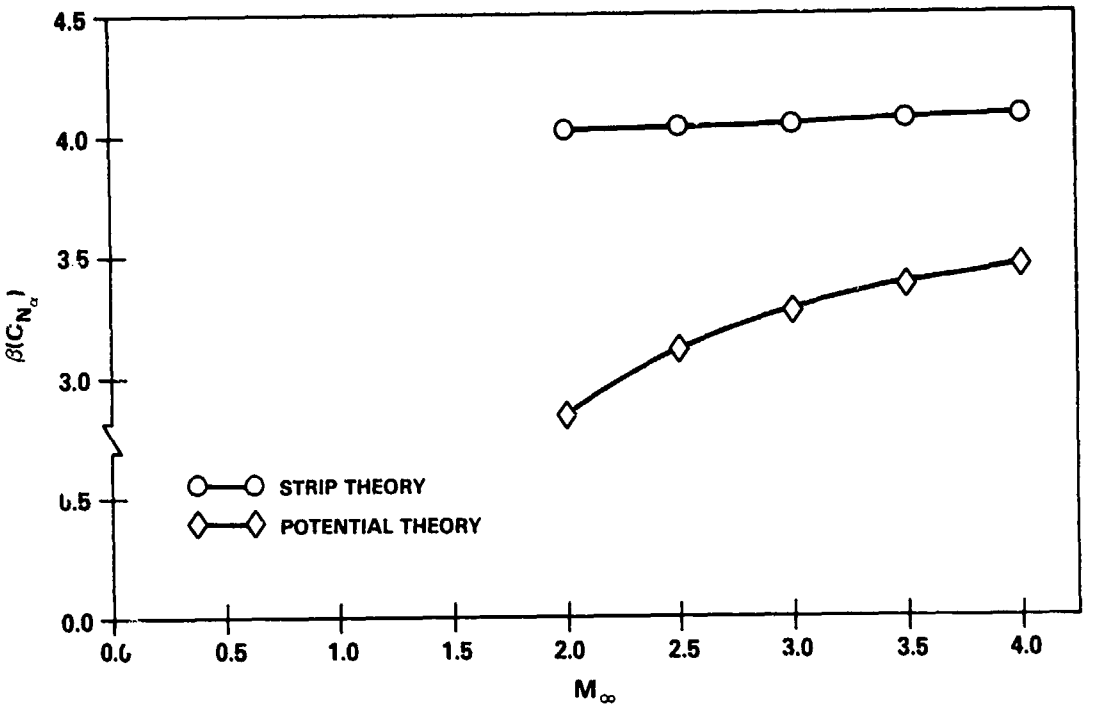


(a) $\lambda_W = 0.99$, $A_W = 1$, $\Lambda_1 = 1°$

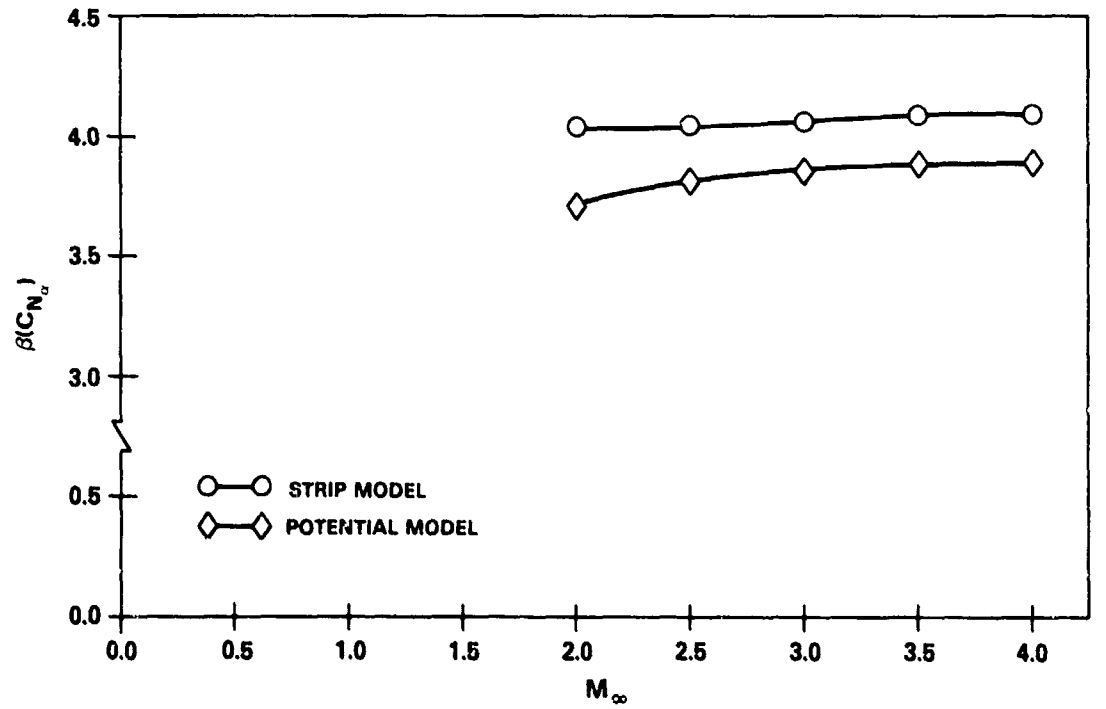


(b) $\lambda_W = 1/3$, $A_W = 2$, $\Lambda_1 = 45°$

Figure 9. $C_{N\alpha}$ Comparison for a Wing

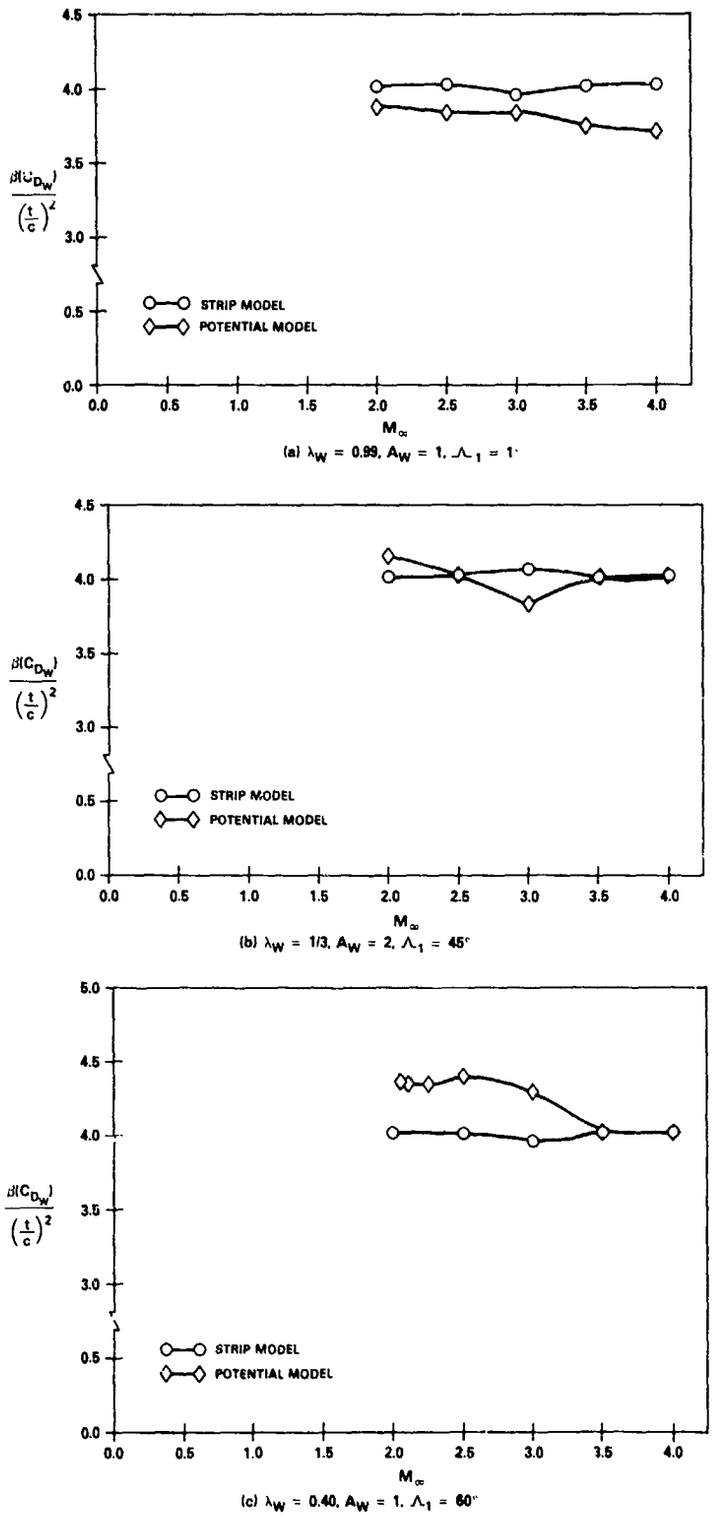


Figure 10. $C_{Dw}$ Comparison for a Wing

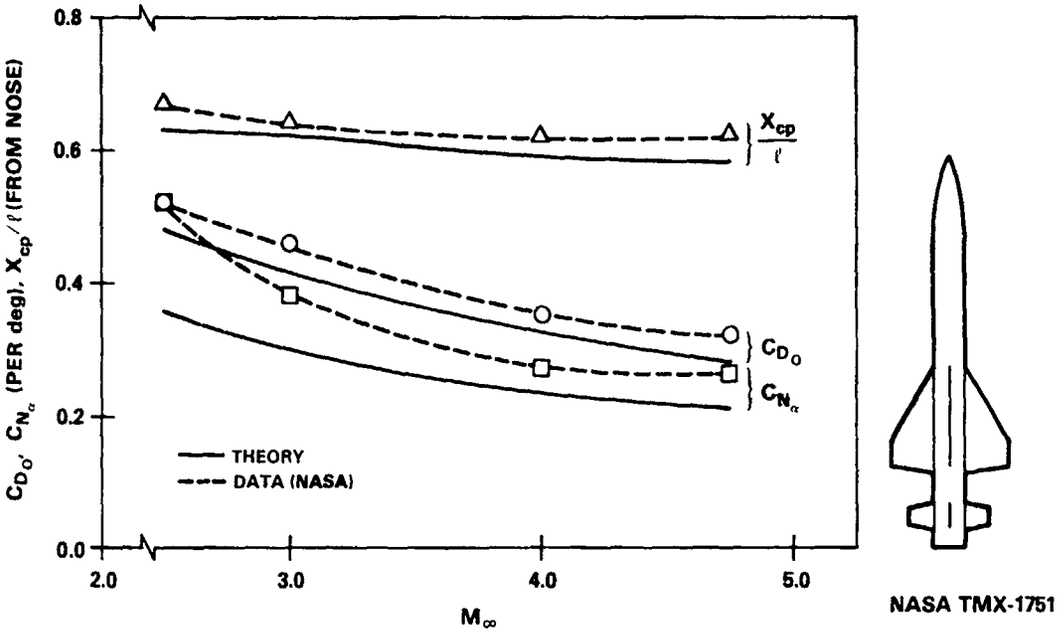


Figure 11. Comparison of Static Aerodynamics for Finned Body at High Mach Numbers ($\alpha = 0°$)

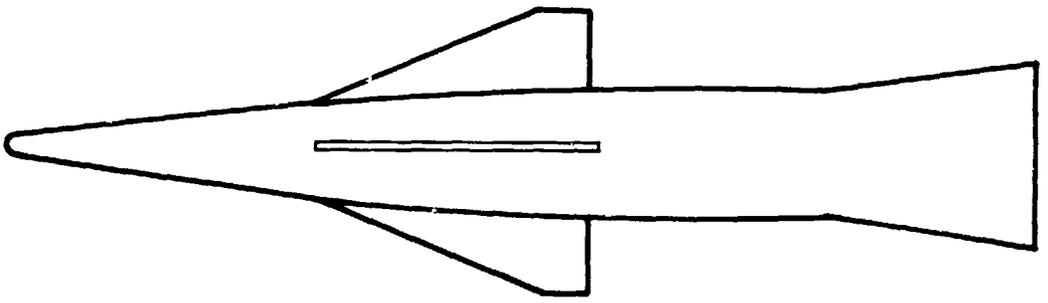

| | $C_{DO}$ | $C_{N\alpha}$ (PER rad) | $X_{cp}/\ell$ (FROM NOSE) |
|---|---|---|---|
| THEORY | 0.39 | 8.4 | 0.63 |
| DATA (NASA) | 0.36 | 7.7 | 0.59 |

Figure 12. Aerodynamics for TMX-187 ($M_\infty = 4.65$, $\alpha = 0°$)

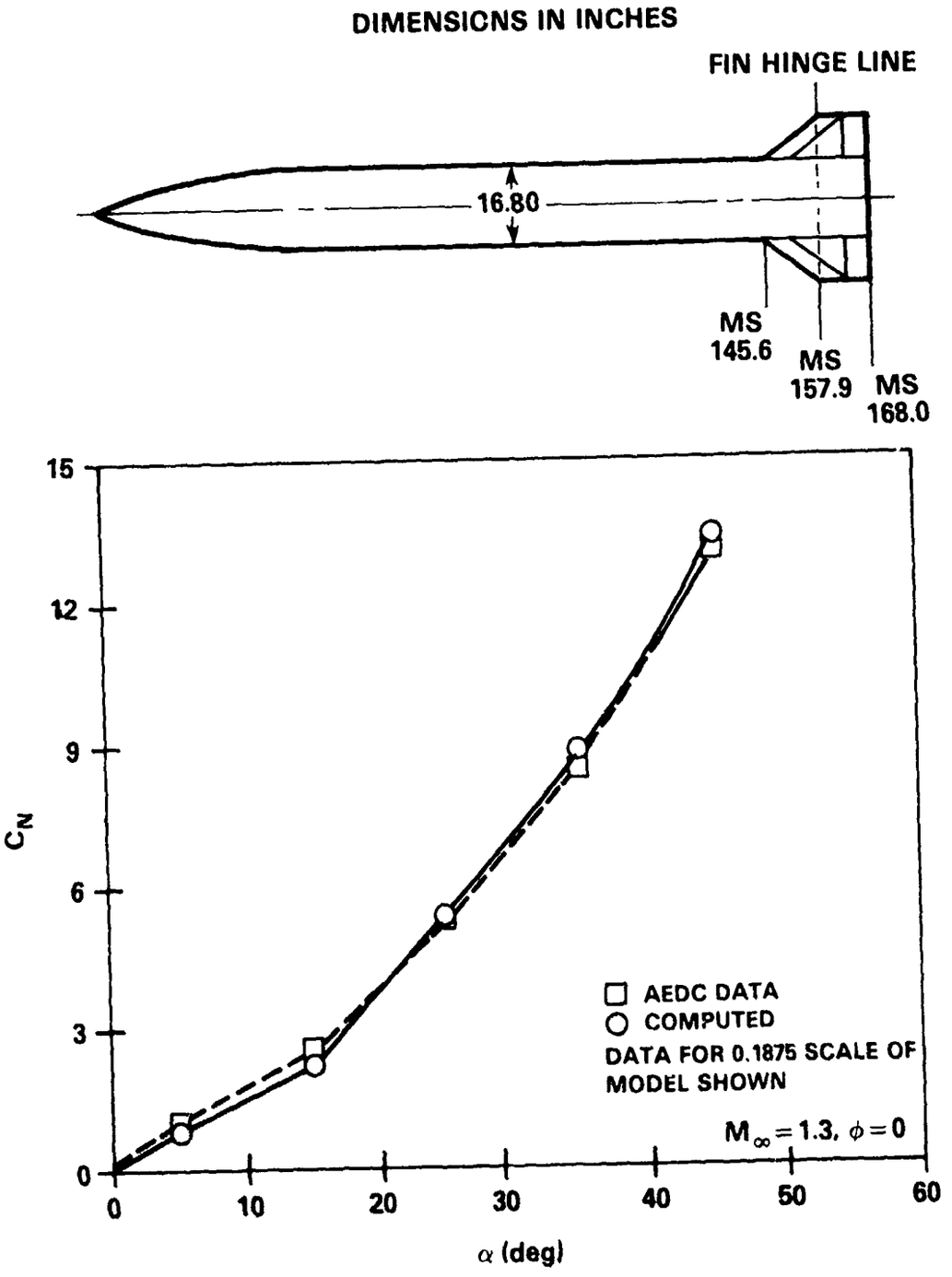


Figure 13. $C_N$ Comparison for Air Slew Demonstrator

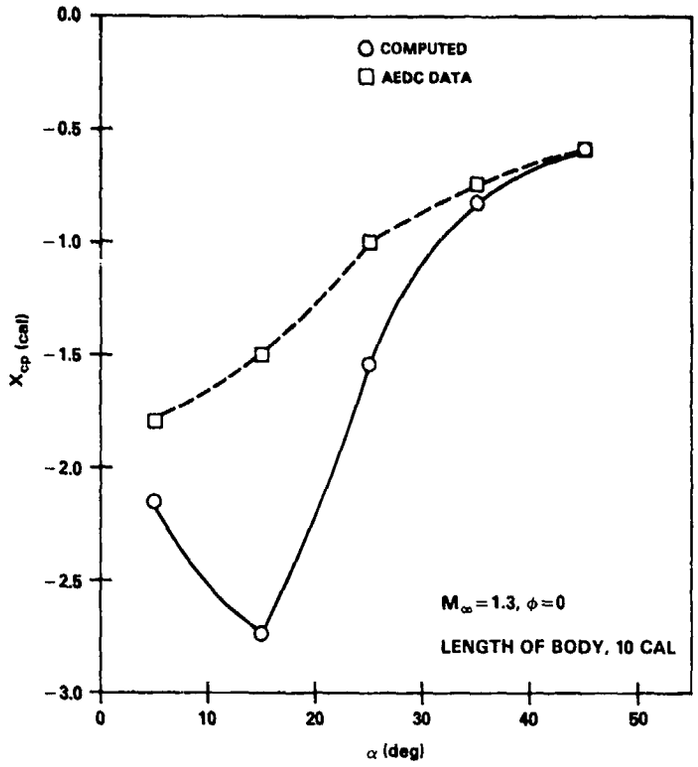


Figure 14. $X_{cp}$ Comparison for Air Slew Demonstrator Forward of Body Midpoint

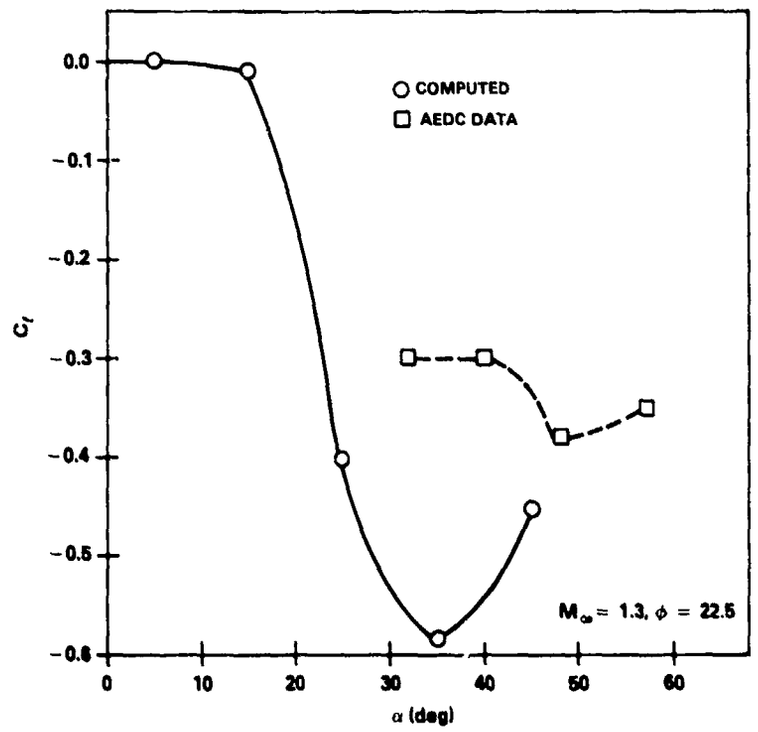


Figure 15. $C_\ell$ Comparison for Air Slew Demonstrator

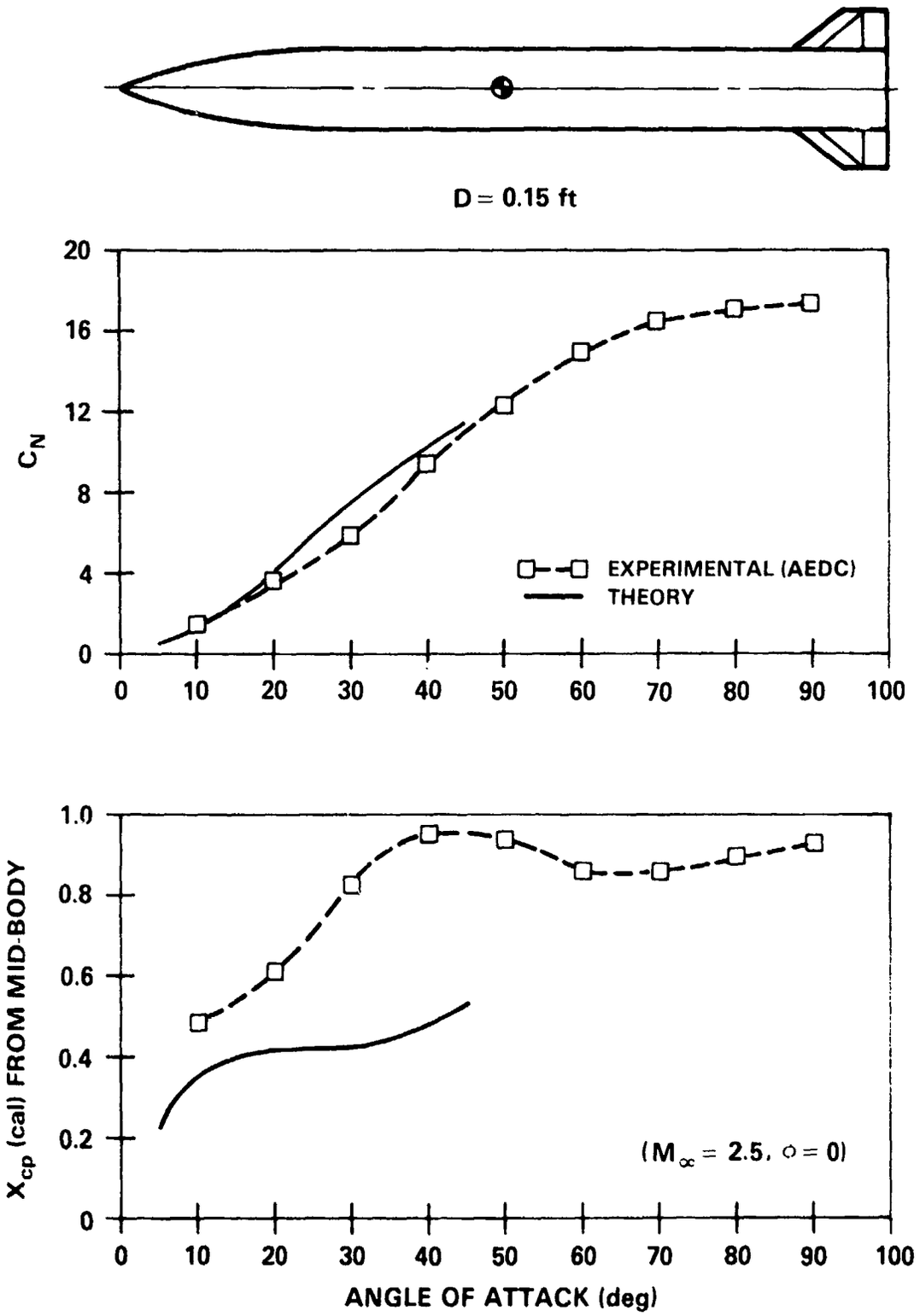


Figure 16. Modified Basic Finner Aerodynamic Comparison

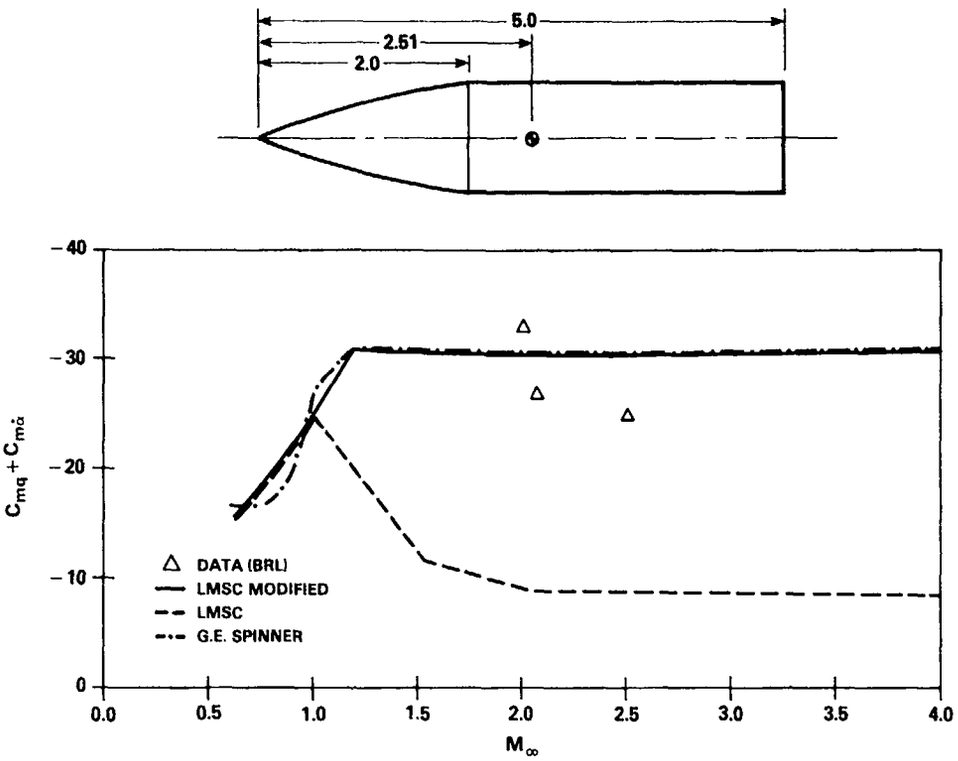


Figure 17. Army-Navy Spinner Pitch Damping Comparison

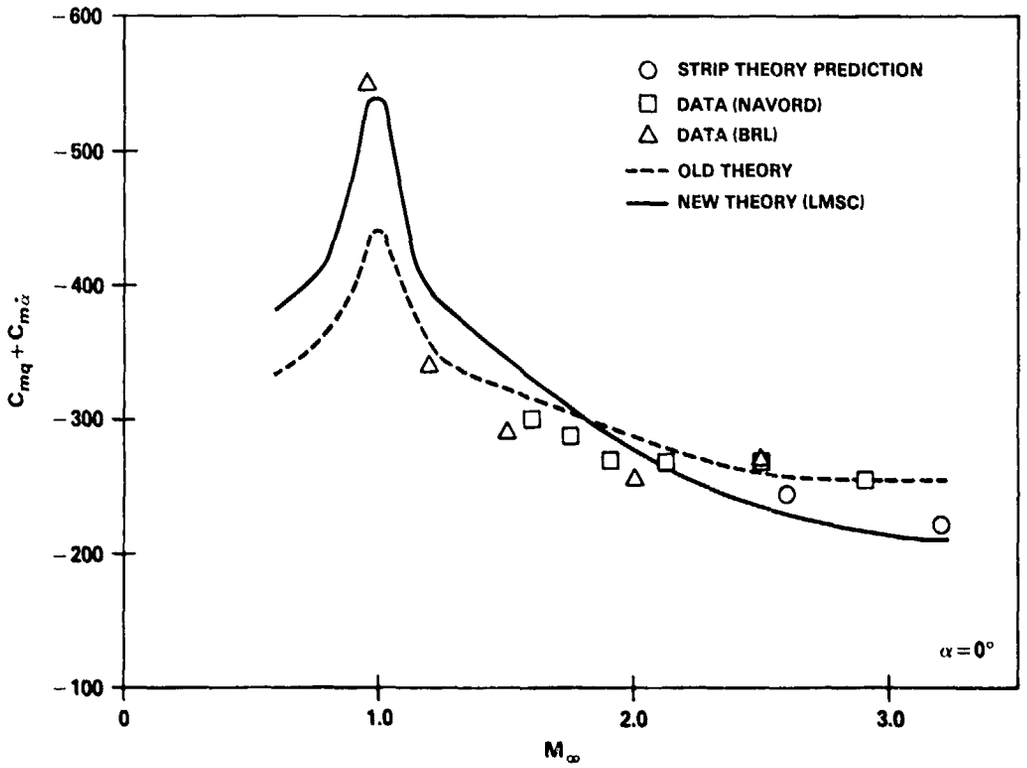


Figure 18. Basic Finner Pitch Damping Comparison

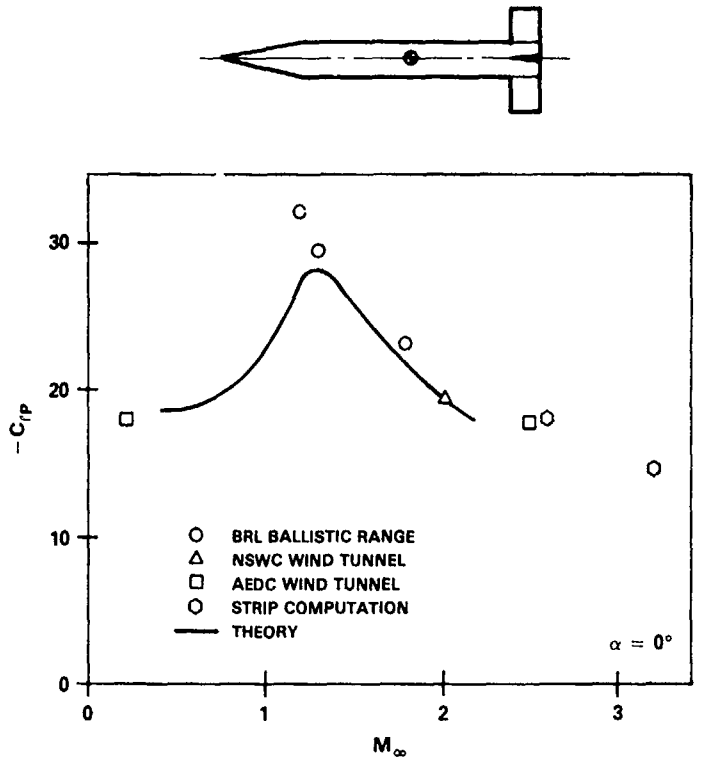


Figure 19. $C_{\ell p}$ Comparison for Army-Navy Basic Finner

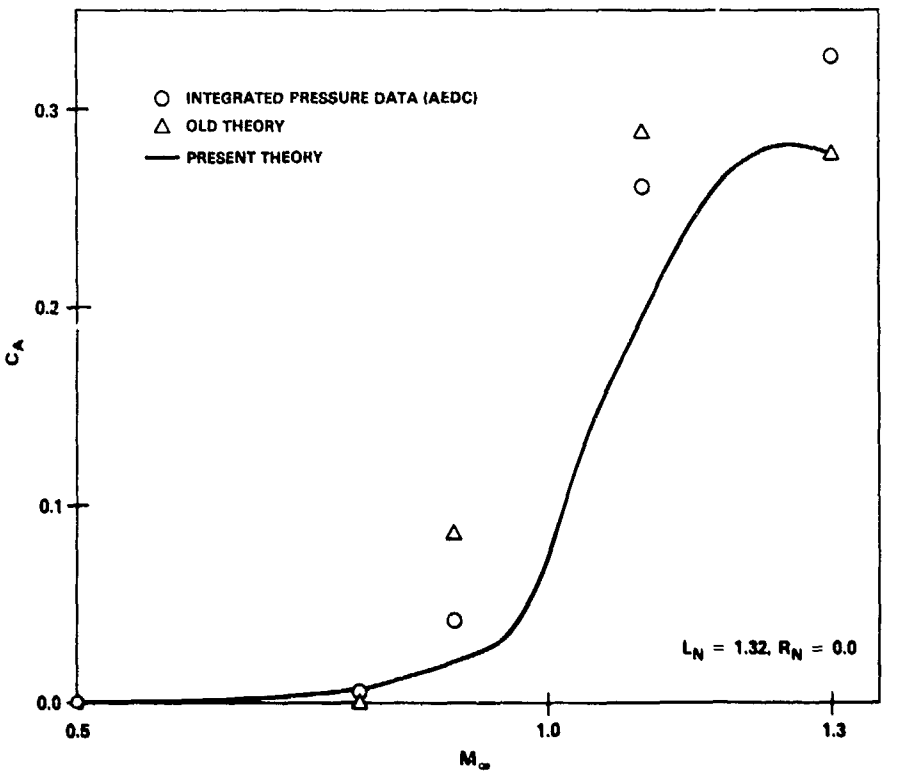


Figure 20. M-117 Bomb Nose Wave Drag Comparison

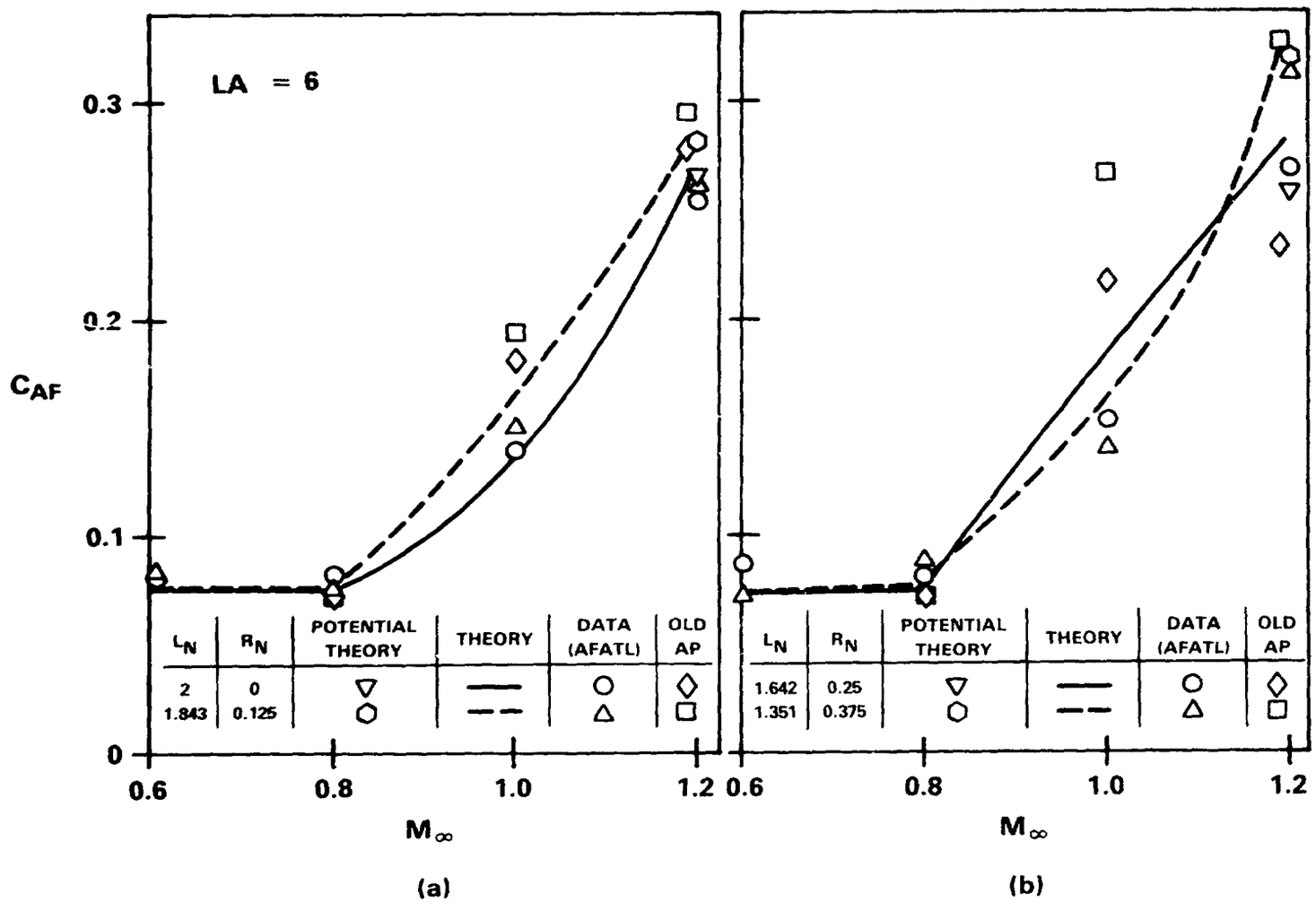


Figure 21. $C_{AF}$ Comparison for Blunted Tangent Ogive-Cylinders

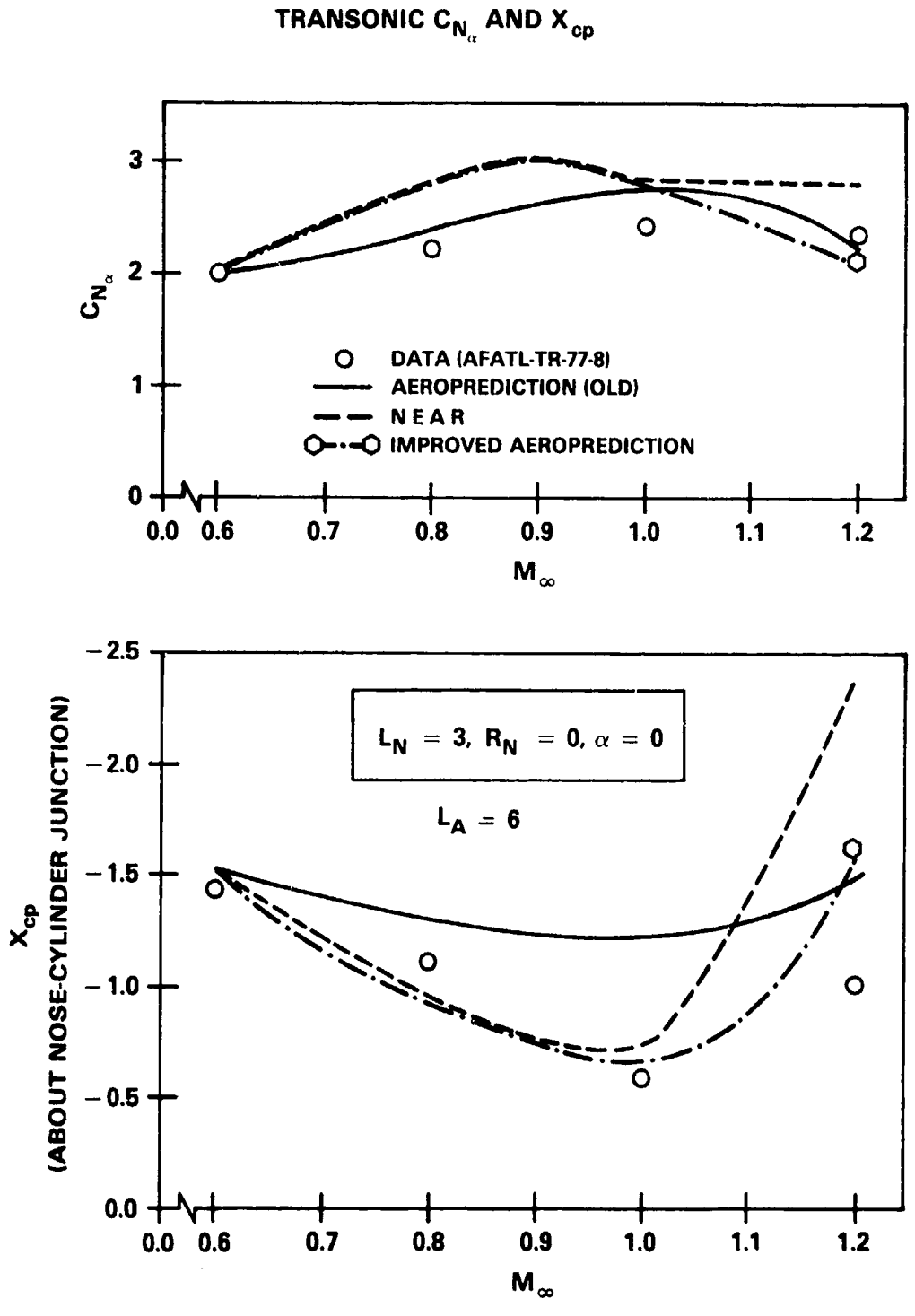


Figure 22. $C_{N\alpha}$ and $X_{cp}$ Comparison for Blunted Tangent Ogive-Cylinders

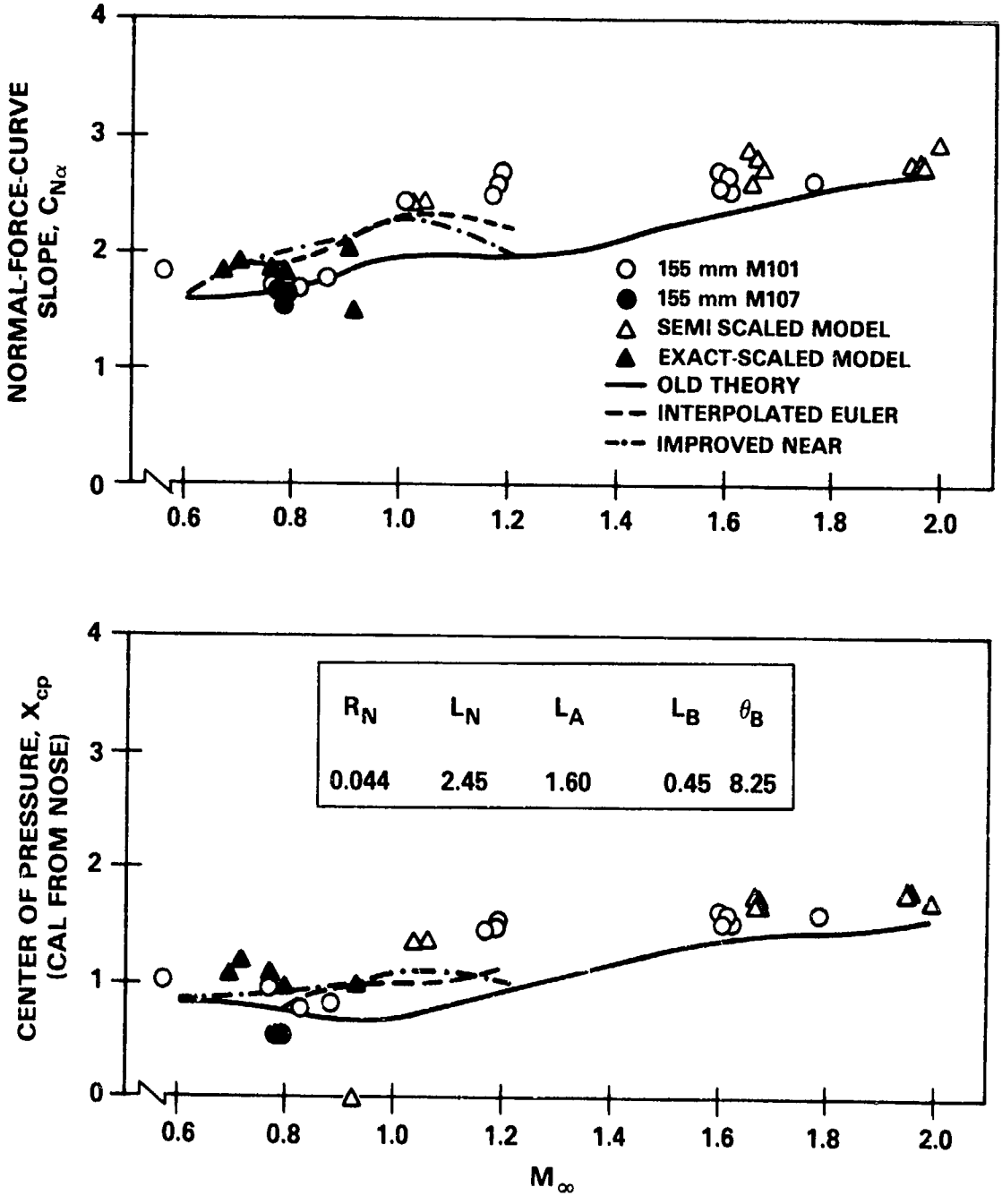


Figure 23. Comparison of Theory and Test Data for 155 mm Projectile

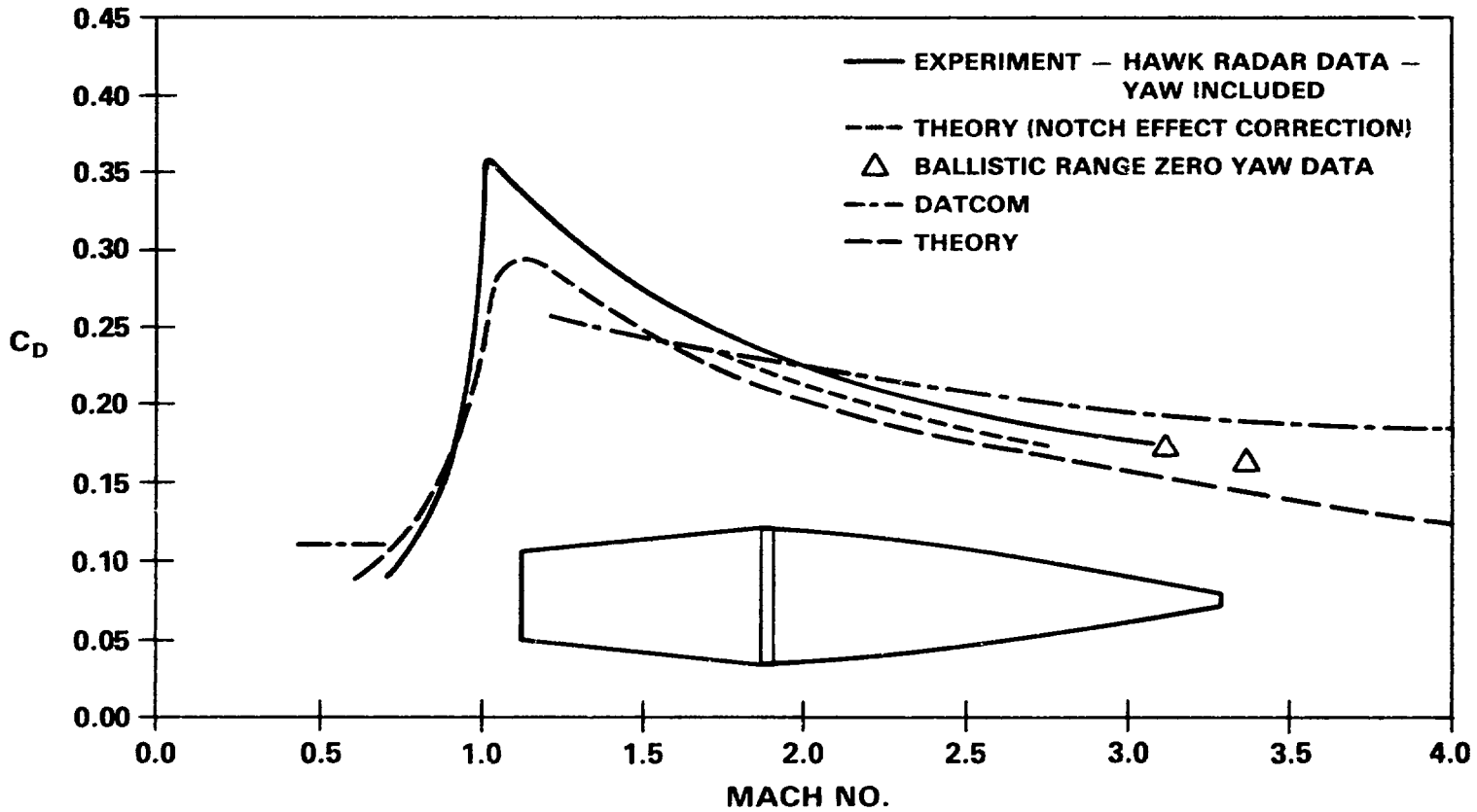


Figure 24. Static Aerodynamics for 30 mm Air Defense Projectile Using the Aeroprediction Code

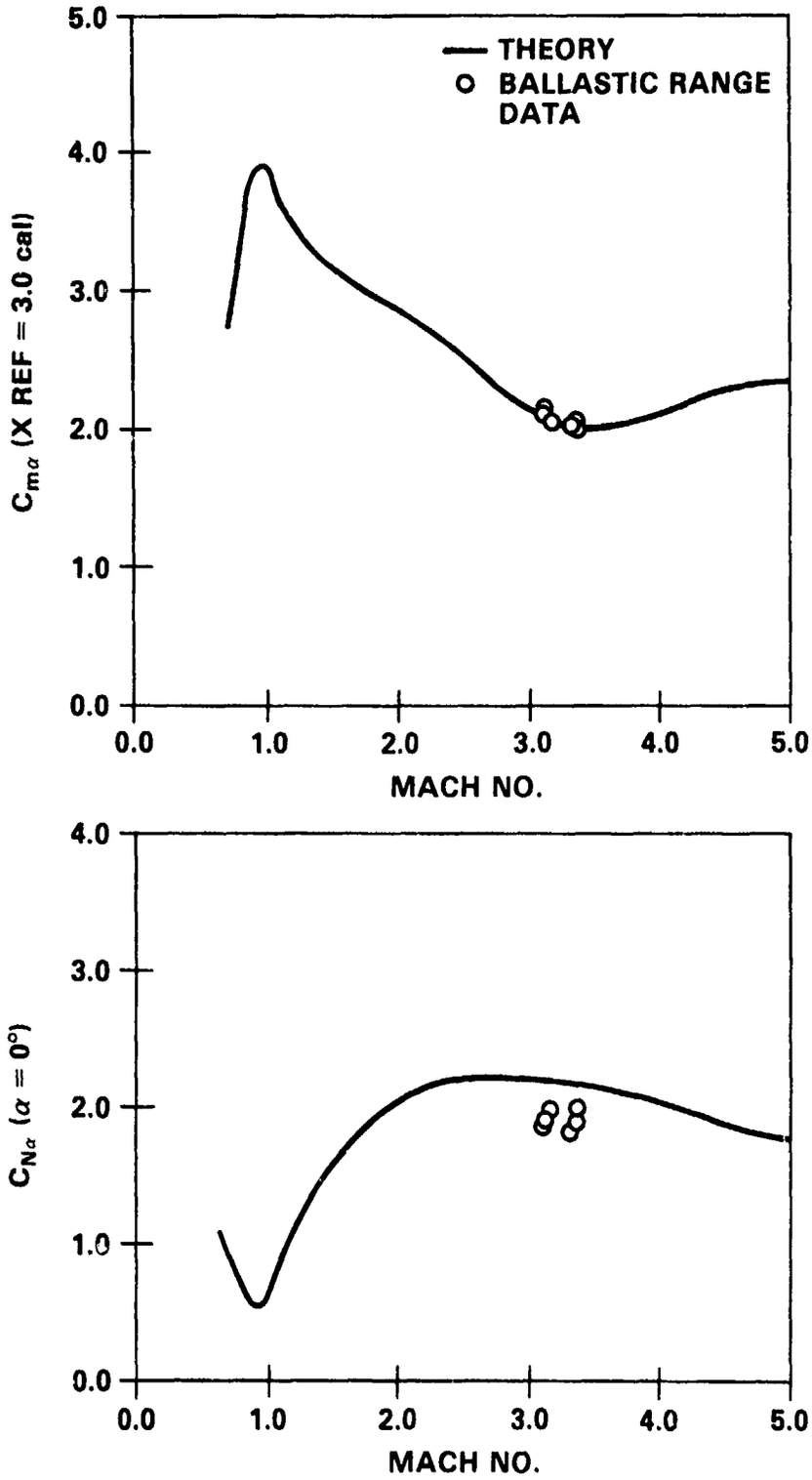


Figure 24 (cont.). Static Aerodynamics for 30 mm Air Defense Projectile Using the Aeroprediction Code

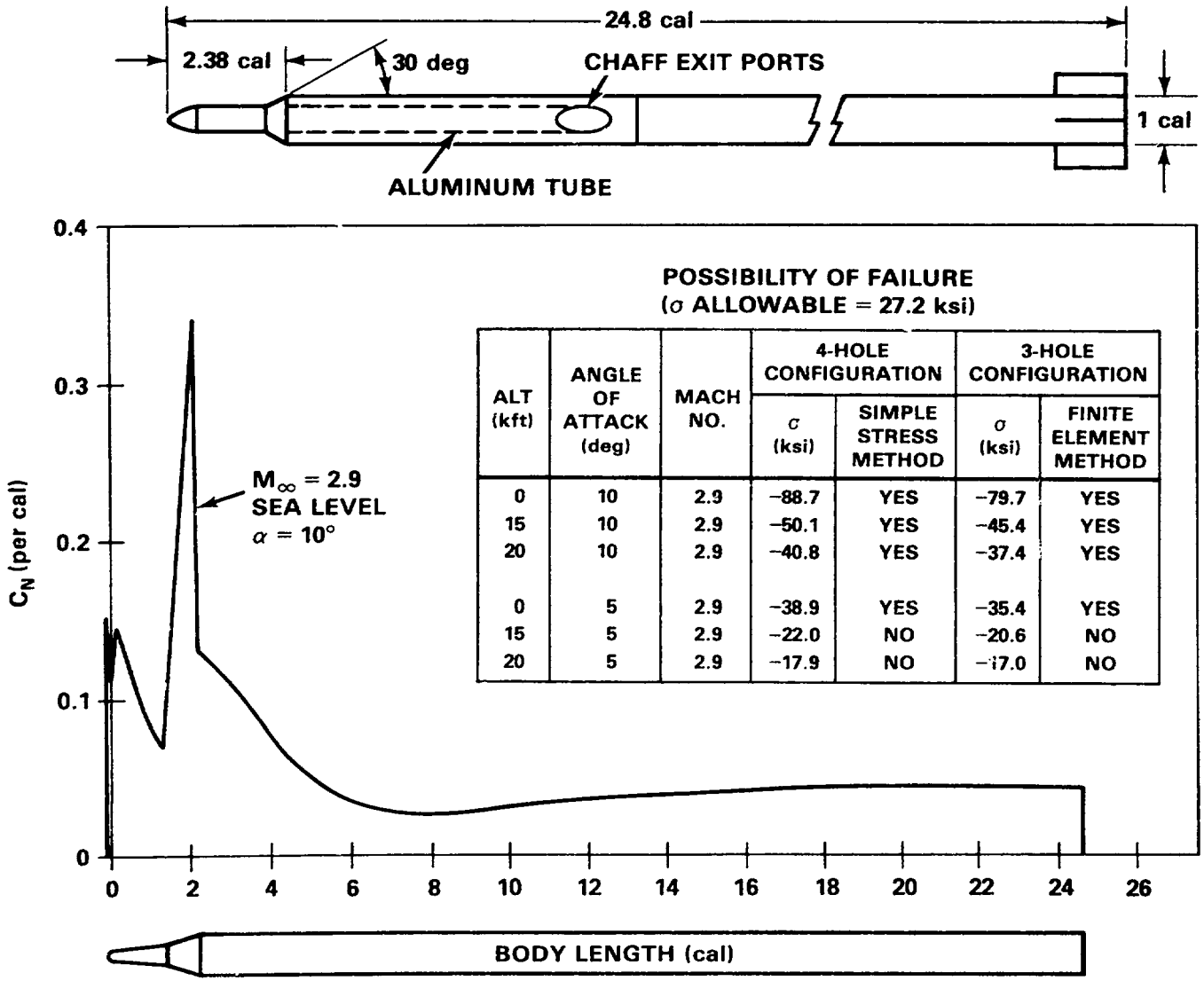


POSSIBILITY OF FAILURE
($\sigma$ ALLOWABLE = 27.2 ksi)

| ALT (kft) | ANGLE OF ATTACK (deg) | MACH NO. | 4-HOLE CONFIGURATION | | 3-HOLE CONFIGURATION | |
|---|---|---|---|---|---|---|
| | | | $\sigma$ (ksi) | SIMPLE STRESS METHOD | $\sigma$ (ksi) | FINITE ELEMENT METHOD |
| 0 | 10 | 2.9 | −88.7 | YES | −79.7 | YES |
| 15 | 10 | 2.9 | −50.1 | YES | −45.4 | YES |
| 20 | 10 | 2.9 | −40.8 | YES | −37.4 | YES |
| 0 | 5 | 2.9 | −38.9 | YES | −35.4 | YES |
| 15 | 5 | 2.9 | −22.0 | NO | −20.6 | NO |
| 20 | 5 | 2.9 | −17.9 | NO | −17.0 | NO |

Figure 25. Structural Integrity Study Using the Aeroprediction Code

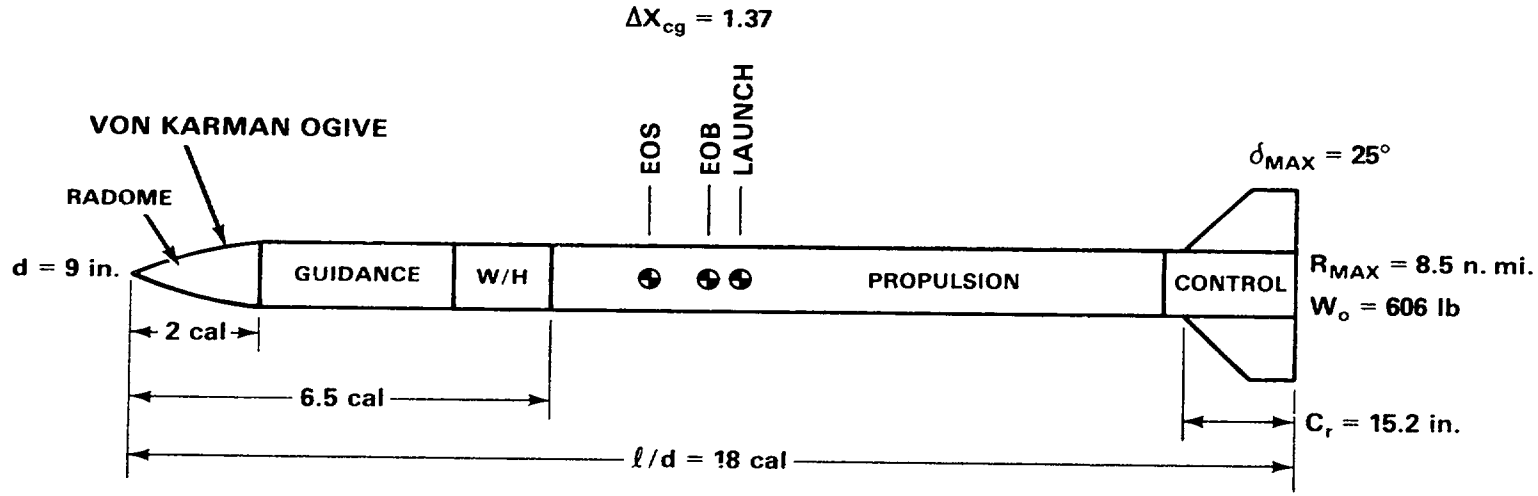


Figure 26. Advanced Point Defense System (APODS) Concept

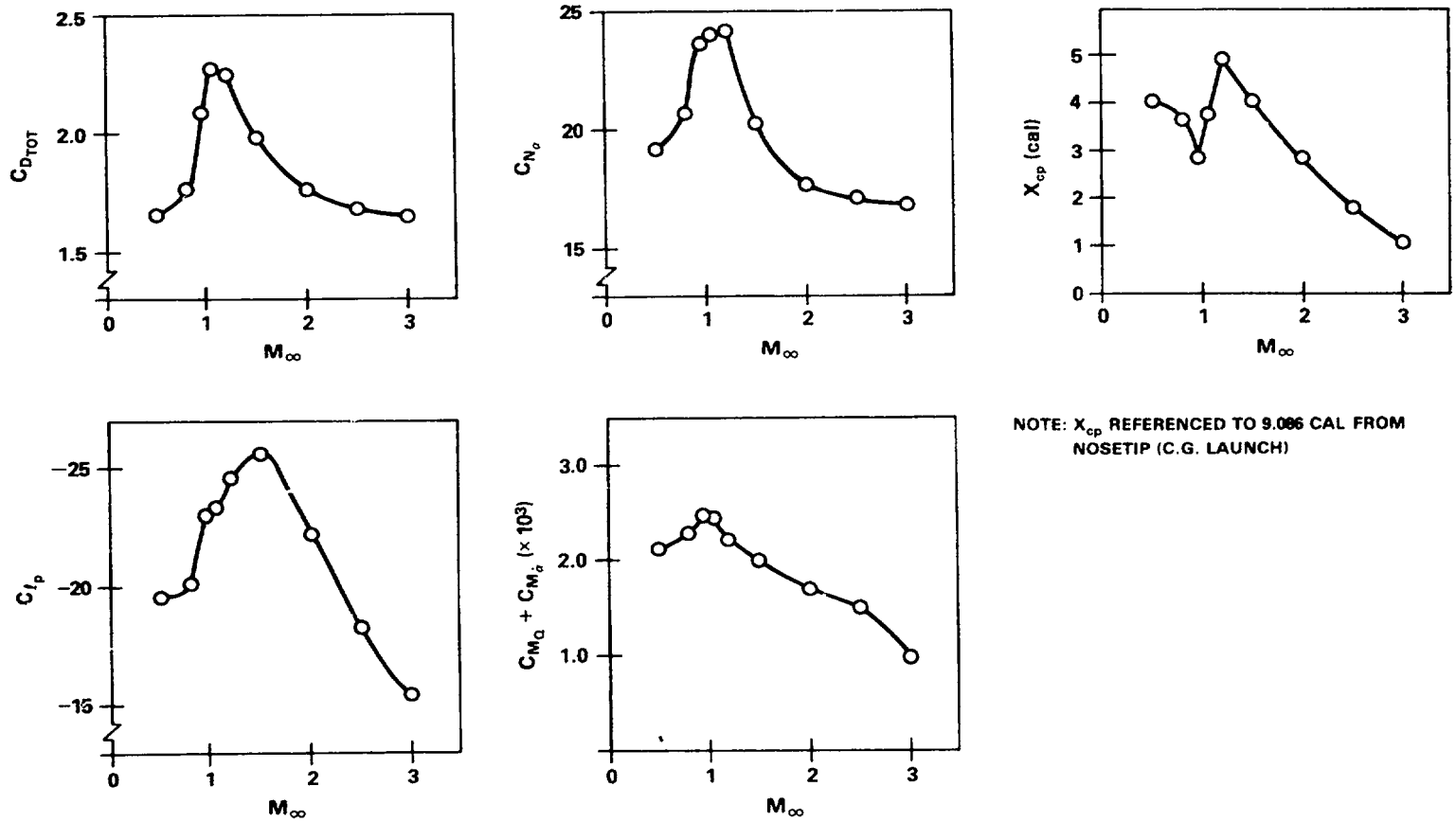


Figure 27. APODS Predicted Aerodynamics Using Aeroprediction Code ($\alpha$ = 15°)

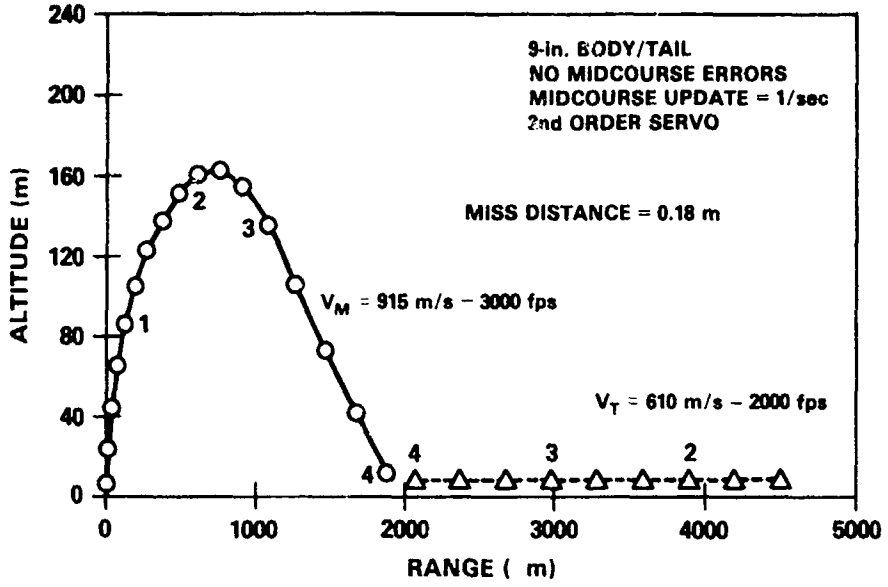


Figure 28. Sample APCDS Performance Trajectory

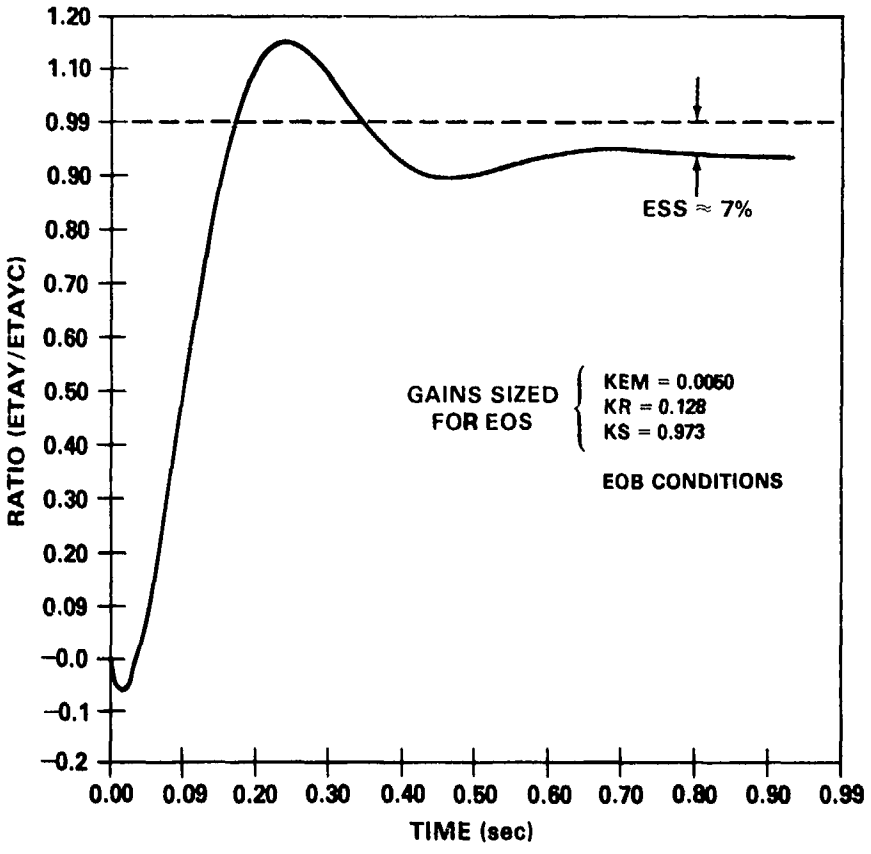


Figure 29. Sample APODS Tail Control Autopilot Response